MOX–Report No. 17/2014

Interface Control Domain Decomposition (ICDD) Method for Stokes-Darcy coupling

Discacciati, M.; Gervasio, P.; Quarteroni, A.

MOX, Dipartimento di Matematica "F. Brioschi"
Politecnico di Milano, Via Bonardi 9 - 20133 Milano (Italy)

mox@mate.polimi.it http://mox.polimi.it

INTERFACE CONTROL DOMAIN DECOMPOSITION (ICDD) METHOD FOR STOKES-DARCY COUPLING *

MARCO DISCACCIATI†, PAOLA GERVASIO‡, AND ALFIO QUARTERONI§

Abstract. We propose the ICDD method to solve the coupling between Stokes and Darcy equations. According to this approach, the problem is formulated as an optimal control problem whose control variables are the traces of the velocity and the pressure on the internal boundaries of the subdomains that provide an overlapping decomposition of the original computational domain. A theoretical analysis is carried out, an efficient solution algorithm is proposed, and several numerical tests are implemented. Our results show the accuracy of the ICDD methos, its computational efficiency and robustness with respect to the different parameters involved (grid-size, polynomial degrees, permeability of the porous domain, thickness of the overlapping region). The ICDD approach is more versatile and easier to implement than the model based on the Beavers, Joseph and Saffman coupling conditions.

Key words. Domain decomposition, Optimal control, Stokes Darcy coupling, Heterogeneous problems, ICDD.

AMS subject classifications. 49K20, 65N30, 65N35, 65N55, 76D07, 76S05

1. Introduction.

Flow processes in a free-fluid region adjacent to a porous medium occur in many relevant applications. To quote some examples, in the filtration of blood through arterial vessel walls and/or body tissues, in industrial processes involving, e.g., air or oil filters and fuel cells, in cross-flow filtration procedures, in the percolation of waters of hydrological basins through rocks and sand, etc.

At the microscopic scale the complete process can in principle be modelled by the Navier-Stokes equations in the whole domain (both in the free-fluid and in the porous medium regions). This would allow the computation of the exact velocity and stress fields without resorting to any averaging procedure. However, it would require a detailed description of the porous medium and its computational cost could be prohibitive.

Alternatively, under the (realistic) assumption that the Reynolds number in the porous domain is small, the Navier-Stokes equations could be there upscaled to a macroscopic level and replaced by the Darcy law [14], the simplest linear relation between the fluid velocity and the pressure. Following this approach, the two different flow regimes (the free fluid and the porous- medium flow) must be suitably coupled to correctly describe the physical process of filtration, through transition region. An extensive overview of coupling strategies to be used in this transition layer is presented in [31].

Physical considerations induce to assume to speculate that the thickness of the transition region is $\mathcal{O}(\varepsilon)$, being ε the characteristic length of the pores inside the porous medium. However, in several models such a region is replaced by a virtual (dimensionless) sharp interface.

*Submitted to SIAM Journal on Numerical Analysis. April 2014

†Laboratori de Càlcul Numèric (LaCàN), Departament de Matemàtica Aplicada III (MA3), Universitat Politècnica de Catalunya (UPC BarcelonaTech), Campus Nord UPC - C2, E-08034 Barcelona, Spain (marco.discacciati@upc.edu)

‡DICATAM, Università di Brescia, via Branze 38, I-25123 Brescia, Italy (paola.gervasio@unibs.it)

§ MATHICSE, Chair of Modelling and Scientific Computing, Ecole Polytechnique Fédérale de Lausanne, Station 8, CH-1015 Lausanne, Switzerland (alfio.quarteroni@epfl.ch)

In the latter case, the most popular method used to couple the two regimes consists in imposing a set of three *interface conditions* based on the mass conservation, the balance of normal forces, and the well-known Beavers–Joseph–Saffman (BJS) condition. Beavers–Joseph condition was derived from experimental observations by Beavers and Joseph [3], then simplified by Saffmann [47] and later justified mathematically by Jäger and Mikelić [32, 33] by using homogenization techniques. Other approaches to derive the same condition are based on volume averaging, upscaling, or matched asymptotic expansion techniques (see, e.g., [41, 34, 11]). However, since such relation depends on a coefficient related to the structure of the porous material close to the interface region and to the position of the interface itself, it is not straightforward to be characterized (see, e.g. [33, 48, 9]).
Recently, Chandesris and Jamet [11] obtained velocity and stress interface jump conditions using a two-step scaling approach and matched asymptotic expansions. Their approach improves the characterization of the jump coefficients by explicitely relating the jump parameters to the porosity and permeability profiles in the interface region, as well as to the position of the interface. However, they require solving auxiliary problems at the mesoscale.
Another approach, alternative to using interface conditions, consists in solving the Brinkman equation [5] in the whole domain (that is both in the fluid and in the porous medium). The transition between the two fluid regimes is achieved automatically by varying in a discontinuous way the permeability and the porosity across a sharp interface and by introducing the so-called effective viscosity in the porous medium. No interface conditions are needed in this approach. See [12] and references therein. This technique is very simple to implement and it is widely used in commercial software, however it is very sensitive to the parameters used in the model and some of the quantities involved (e.g., the effective viscosity) are difficult to characterize in practical applications.

Minor attention has given in literature to the case of a transition region with positive and small thickness. In [41, 42], Ochoa-Tapia and Whitaker solve the Stokes equations in the free-fluid domain, the Stokes problem with an additional term featuring a variable porosity inside the transition region, and the Darcy model with Brinkman correction in the porous domain. Their approach produces a jump in the stress but not in the velocity at the two interfaces of the transition region.

In this paper we propose an alternative approach still based on the use of a thin transition region. However, the novelty is that we do not solve any particular equation inside such a region (neither we enforce any matching conditions in it). In fact, our transition region merely represents the overlap of two regions, one in which we solve the free fluid (Stokes) equations, the other where we solve the porous medium (Darcy) equation. The coupling between the two solutions is not modelled, rather it is achieved through a novel strategy based on imposing in a least-squares sense the continuity of velocity and pressure only across the two subdomain interfaces that delimitate the thin transition layer.

More specifically, we use the so-called Interface Control Domain Decomposition (ICDD) method, introduced in [18, 20] as a solution strategy for boundary value problems governed by elliptic partial differential equations and extended to the Stokes equations in [19]. The ICDD method shares some similarities with the classic overlapping Schwarz method [49, 45, 50] and with the Least Square Conjugate Gradient [28] and the Virtual Control [38, 24] methods, and it is characterized by a decomposition of the original domain into overlapping regions.

ICDD method introduces new auxiliary control variables on the subdomain internal boundaries (named interfaces) that play the role of the unknown traces (or fluxes) of the state solutions of the subproblems. Such controls are determined by minimizing a suitable cost functional that measures the jump of the quantities of interest at the interfaces of the decomposition. As a matter of fact we solve an optimal control problem in which both controls and observation are defined on the interfaces and whose constraints are the PDE's on the overlapping subdomains.

The choice of the cost functional is crucial to ensure the uniqueness of the solution on the overlapping area and the correct representation of the physical phenomenon of interest.

In this paper we propose and analyze an ICDD method for the Stokes-Darcy coupling, in which the controls are of Dirichlet type: we control the velocity on the interface of the Stokes domain and the pressure on the interface of the Darcy one. The cost functional measures the gap between Stokes and Darcy velocities on one interface and the gap of the pressures on the other one. In this way, both Stokes and Darcy subproblems are closed by very simple (Dirichlet) boundary conditions on the interfaces and there is no need to evaluate neither fluxes nor tangential derivatives, nor to solve auxiliary problems inside the layer region. In particular, this feature makes ICDD very suitable to deal interfaces of arbitrary shape (not only straight lines).

Preliminary results obtained in the homogeneous elliptic coupling (see [18]) show that if the controls are of Dirichlet type (i.e. the traces of the state variables) and the cost functional measures the jump of the state solutions across the interfaces, then the number of iterations required to solve the optimality system associated with the optimal control problem is independent of the discretization parameters (the mesh size and the polynomial degree in $hp-$FEM context) and, in some circumstances, also of the overlap thickness δ (see [18, 19]). Numerical results presented in this paper show that the same conclusions hold true also for the heterogeneous coupling between Stokes and Darcy equations.

In the case of the Stokes-Darcy coupling the thickness δ of the overlapping region is crucial to correctly represent the filtration process. As we will show in Sect. 6, δ should be set proportional to the characteristic length of the pores ε or, after adimensionalization, to the ratio between ε and the characteristic length x_s of the Stokes domain in the dimensional case. Using a totally different argument, a similar quantity d/h was introduced in the asymptotic expansion of Chandesris and Jamet in [11], where d is proportional to the pore dimension, while h is the height of the fluid standing above the porous layer.

Numerical comparison with the Beavers–Joseph–Saffman condition on a sharp interface shows that ICDD provides accurate solutions for both *near parallel* and *near normal flows* to the porous media, following the classification of Ene, Levy, and Sanchez-Palencia [22, 37].

The outline of the paper is as follows. In section 2 we introduce the physical setting of the filtration problem. In section 3 we present the ICDD method characterizing the cost functional and suitable interface control variables. In section 4 we present the hp-FEM discretization of the optimal control problem, while in section 5 we focus on its mathematical analysis. Finally, section 6 presents several numerical results aimed at studying the convergence behavior of the proposed ICDD methods and at comparing it to the classical coupling strategy relying on the Beavers–Joseph–Saffman interface conditions.

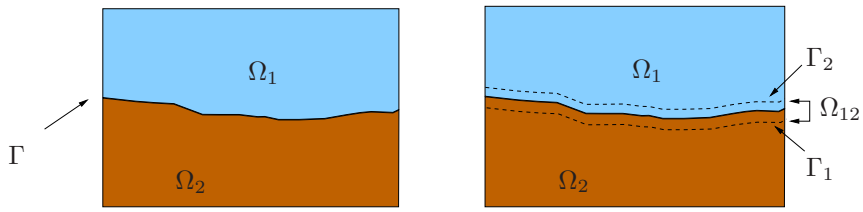

FIG. 2.1. *Representation of a 2D section of a possible computational domain for the coupled free/porous-media flow problem. At left a decomposition with sharp interface* Γ*, at right a decomposition with overlap*

2. Setting. Let $\Omega \subset \mathbb{R}^d$ $(d = 2, 3)$ be an open bounded domain with Lipschitz continuous boundary $\partial\Omega$. It represents the region of our interest that is naturally split into two non-overlapping parts: one, Ω_1, occupied by an incompressible fluid, the other, Ω_2, by a porous medium. The fluid in Ω_1 can filtrate through the adjacent porous medium.

The subdomains Ω_1 and Ω_2 represent a disjoint partition of Ω, that is $\overline{\Omega} = \overline{\Omega}_1 \cup \overline{\Omega}_2$ and $\Omega_1 \cap \Omega_2 = \emptyset$. We denote by $\Gamma = \partial\Omega_1 \cap \partial\Omega_2$ the nominal physical interface between these two subregions, as shown in the left picture of Fig. 2.1. We make the assumption that Γ is regular enough to ensure that both $\partial\Omega_1$ and $\partial\Omega_2$ are Lipschitz continuous too. Then, let $(0, T)$ denote a suitable time interval.

For simplicity, we assume that the fluid domain is confined, i.e., we neglect here the case of free-surface flows, hence the subdomains Ω_1 and Ω_2 do not change in the time interval.

The free/porous-media flow problem is modeled by the coupling of Navier-Stokes equations and Darcy law (see, e.g., [40, 21, 17]).

More precisely, the fluid satisfies the incompressible Navier-Stokes equations in the free-fluid domain

$$\begin{array}{ll} \rho\partial_t \mathbf{u}_1 - \nabla \cdot \mathbf{T}_1(\mathbf{u}_1, p_1) + \rho(\mathbf{u}_1 \cdot \nabla)\mathbf{u}_1 = \mathbf{f}_1 & \text{in } \Omega_1 \times (0, T) \\ \nabla \cdot \mathbf{u}_1 = 0 & \text{in } \Omega_1 \times (0, T) \end{array} \tag{2.1}$$

where $\mathbf{u}_1 = \mathbf{u}_1(\mathbf{x}, t)$ and $p_1 = p_1(\mathbf{x}, t)$ denote, respectively, the velocity and the pressure of the free fluid in $\Omega_1 \times (0, T)$;

$$\mathbf{T}_1(\mathbf{u}_1, p_1) = \mu(\nabla \mathbf{u}_1 + (\nabla \mathbf{u}_1)^T) - p_1 \mathbf{I} \tag{2.2}$$

is the Cauchy stress tensor, where $\mu > 0$ and $\rho > 0$ are the dynamic viscosity and the density of the fluid; finally $\mathbf{f}_1 \in [L^2(\Omega_1 \times (0, T))]^d$ is a given external force.

Inside the porous domain the fluid obeys the Darcy law ([2])

$$\mathbf{u}_2 = -\mathbf{K}\nabla\varphi_2 \qquad \text{in } \Omega_2 \times (0, T), \tag{2.3}$$

where $\mathbf{u}_2 = \mathbf{u}_2(\mathbf{x}, t)$ is the specific discharge (also known as Darcy velocity, seepage velocity, filtration velocity, or volumetric flux density) and represents the average of the fluid velocity over a volume element of the medium (incorporating both solid and fluid material); $\varphi_2 = \varphi_2(\mathbf{x}, t)$ is the piezometric head, while $\mathbf{K} = \mathbf{K}(\mathbf{x})$ is the *hydraulic conductivity* and it is a symmetric positive definite tensor whose components k_{ij} belong to $L^\infty(\Omega_2)$ and, dimensionally speaking, represent velocities.

The hydraulic conductivity tensor depends on both the density ρ and the dynamic viscosity μ of the fluid, as well as on the intrinsic permeability $\boldsymbol{\kappa} = \boldsymbol{\kappa}(\mathbf{x})$ of the media

as follows:

$$\mathbf{K} = \frac{\boldsymbol{\kappa}}{\mu}\rho g. \tag{2.4}$$

The piezometric head is related to the intrinsic average pressure $p_2 = p_2(\mathbf{x}, t)$ of the fluid inside the porous media, i.e.

$$\varphi_2 = (z - z_0) + \frac{1}{\rho g}p_2 \qquad \text{in } \Omega_2 \times (0, T), \tag{2.5}$$

where $z - z_0$ is the elevation with respect to a reference quote z_0.

The Darcy velocity $\mathbf{u}_2$ inside the porous media satisfies the incompressibility constraint

$$\nabla \cdot \mathbf{u}_2 = 0 \qquad \text{in } \Omega_2 \times (0, T). \tag{2.6}$$

In view of (2.4) and (2.5), the Darcy law (2.3) reads also

$$\mathbf{u}_2 = -\frac{\boldsymbol{\kappa}}{\mu}\nabla(p_2 + \rho g(z - z_0)) \qquad \text{in } \Omega_2 \times (0, T). \tag{2.7}$$

Denoting by $\hat{p} = -\rho g(z - z_0)$ the *hydrostatic pressure*, the function

$$\tilde{p}_2 = p_2 - \hat{p} = p_2 + \rho g(z - z_0) \tag{2.8}$$

is in fact the *hydrodinamic pressure* of the fluid inside the porous domain. The same splitting can be performed in the fluid domain, i.e. $\tilde{p}_1 = p_1 - \hat{p}$.

We recall that the Darcy model is meaningful either when the characteristic length scale of the pores (ε) is very small with respect to the characteristic length x_s of the Stokes domain, or when the Reynolds number $\mathrm{Re}_\varepsilon = \varepsilon^3\langle\nabla p_2\rangle\rho/\mu$ in the Darcy domain is small with respect to 1 (here $\langle\nabla p_2\rangle$ denotes the average of the pressure gradient on a representative volume element in Ω_2; see [22]).

A commonly used set of interface conditions to couple (2.1) and (2.3) across the sharp interface Γ reads [21]:

$$\begin{array}{ll} \mathbf{u}_1 \cdot \mathbf{n} = \mathbf{u}_2 \cdot \mathbf{n} & \text{on } \Gamma \times (0, T) \\ -(\mathbf{T}_1(\mathbf{u}_1, p_1)\mathbf{n}) \cdot \mathbf{n} = p_2 & \text{on } \Gamma \times (0, T) \\ -(\mathbf{T}_1(\mathbf{u}_1, p_1)\mathbf{n}) \cdot \boldsymbol{\tau} = \dfrac{\alpha_{BJ}\mu}{\sqrt{\boldsymbol{\tau}^T\boldsymbol{\kappa}\boldsymbol{\tau}}}\mathbf{u}_1 \cdot \boldsymbol{\tau} & \text{on } \Gamma \times (0, T) \end{array} \tag{2.9}$$

where $\mathbf{n}$ is the normal unit vector to Γ directed outward of Ω_1, $\boldsymbol{\tau}$ represents a set of linear independent unit tangential vectors to Γ with $\boldsymbol{\tau} \cdot \mathbf{n} = 0$, and α_{BJ} is a dimensionless coefficient depending on the geometrical characteristics of the porous medium.

Condition $(2.9)_1$ is a consequence of the conservation of mass across the interface; $(2.9)_2$ is due to the balance of normal forces (see, e.g., [15, 27, 36]); while $(2.9)_3$ is the so-called *Beavers–Joseph–Saffman* interface condition [3, 47, 32, 36, 15, 46] that establishes proportionality between the tangential component of the flux and that of the free velocity. (Note that $(2.9)_3$ is not a coupling condition.)

It is well known that $(2.9)_3$ is meaningful when the Darcy velocity is negligible with respect to the Navier-Stokes velocity at the interface, otherwise it must be replaced by the more complete Beavers–Joseph (coupling) condition (see [3, 35])

$$-(\mathbf{T}_1(\mathbf{u}_1, p_1)\mathbf{n}) \cdot \boldsymbol{\tau} = \frac{\alpha_{BJ}\mu}{\sqrt{\boldsymbol{\tau}^T\boldsymbol{\kappa}\boldsymbol{\tau}}}(\mathbf{u}_1 - \mathbf{u}_2) \cdot \boldsymbol{\tau} \qquad \text{on } \Gamma \times (0, T). \tag{2.10}$$

The global nonlinear coupled Navier-Stokes/Darcy problem is defined by (2.1), (2.6), (2.7) and (2.9) suitably completed with initial and boundary conditions.

The mathematical analysis of the steady Navier-Stokes/Darcy problem can be found in [21, 27], while the unsteady case has been studied in [10]. In [21, 1] the authors propose and analyze substructuring iterative domain decomposition methods to efficiently solve the coupled problem. In particular, Dirichlet-Neumann and Robin-Robin methods are studied for the steady Stokes/Darcy case (see also [16]), while Newton methods are proposed for the steady Navier-Stokes/Darcy one.

A linearization of the coupled problem can be obtained by replacing the Navier-Stokes momentum equation $(2.1)_1$ by the Oseen one, that reads:

$$\rho\partial_t\mathbf{u}_1 - \nabla\cdot\mathbf{T}_1(\mathbf{u}_1,p_1) + \rho(\mathbf{u}^*\cdot\nabla)\mathbf{u}_1 = \mathbf{f}_1 \quad \text{in } \Omega_1\times(0,T). \tag{2.11}$$

If $\mathbf{u}^*=\mathbf{0}$, (2.11) is nothing else than the Stokes equation; the non-linear term is dropped and this replacement is justified when the Reynolds number of the fluid is low, i.e., in case of slow motion of fluids with high viscosity. This linearized problem is also interesting since a steady Stokes problem can be generated when considering a semi-implicit time discretization of the Navier-Stokes equations where all terms but the non-linear convective one have been dealt with implicitly.

In the more general case (when $\mathbf{u}^*\neq\mathbf{0}$) the convective term is maintained, but the non-linearity is eliminated by replacing $\mathbf{u}_1=\mathbf{u}_1(\mathbf{x},t)$ with a suitable approximation $\mathbf{u}^*=\mathbf{u}^*(\mathbf{x},t)$ that can be explicitly computed by using the evaluatation of $\mathbf{u}_1$ at previous time-steps.

In view of these considerations, from now on we focus on the steady linear momentum equation

$$-\nabla\cdot\mathbf{T}_1(\mathbf{u}_1,p_1) + \alpha\mathbf{u}_1 = \mathbf{f}_1 \quad \text{in } \Omega_1 \tag{2.12}$$

instead of $(2.1)_1$. The zeroth order term $\alpha\mathbf{u}_1$, with $\alpha>0$ arises from the discretization of the temporal derivative by a classic finite difference scheme.

3. ICDD method. We consider an overlapping decomposition of the computational domain Ω in two subdomains Ω_1 and Ω_2 such that

$$\overline{\Omega}=\overline{\Omega}_1\cup\overline{\Omega}_2, \quad \Omega_{12}=\Omega_1\cap\Omega_2\neq\emptyset, \quad \Gamma_i=\partial\Omega_i\setminus\partial\Omega,\ i=1,2, \tag{3.1}$$

as shown in the right picture of Figure 2.1. We consider a formulation based on ICDD method that was already proposed and analyzed in [18, 20] for elliptic problems and in [19] for Stokes equations.

For $i=1,2$, let $\partial\Omega_i^N$ and $\partial\Omega_i^D$ be non-empty, non-intersecting and complementary subsets of $\partial\Omega_i\cap\partial\Omega$; $\mathbf{n}_i$ be the unit normal vector to $\partial\Omega_i$ directed outwards the domain Ω_i. For the sake of simplicity and without loosing generality, we consider homogeneous boundary conditions on $\partial\Omega$.

The ICDD method for the Stokes/Darcy problem consists in introducing unknown functions $\boldsymbol{\lambda}_1$ and λ_2 defined on the interfaces Γ_1 and Γ_2, respectively, that are named *controls* and play the role of Dirichlet data for the following Stokes and Darcy subproblems, respectively:

$$\text{Stokes system:}\quad \begin{array}{ll} -\nabla\cdot\mathbf{T}_1(\mathbf{u}_1,p_1)+\alpha\mathbf{u}_1=\mathbf{f}_1 & \text{in } \Omega_1\\ \nabla\cdot\mathbf{u}_1=0 & \text{in } \Omega_1\\ \mathbf{u}_1=\boldsymbol{\lambda}_1 & \text{on } \Gamma_1\\ \mathbf{u}_1=\mathbf{0} & \text{on } \partial\Omega_1^D\\ \mathbf{T}_1(\mathbf{u}_1,p_1)\mathbf{n}_1=\mathbf{0} & \text{on } \partial\Omega_1^N \end{array} \tag{3.2}$$

$$\text{Darcy system:}\quad \begin{array}{ll} \boldsymbol{\alpha}^{-1}\mathbf{u}_2+\nabla p_2=\mathbf{f}_2 & \text{in } \Omega_2\\ \nabla\cdot\mathbf{u}_2=0 & \text{in } \Omega_2\\ p_2=\lambda_2 & \text{on } \Gamma_2\\ p_2=0 & \text{on } \partial\Omega_2^D\\ \mathbf{u}_2\cdot\mathbf{n}_2=0 & \text{on } \partial\Omega_2^N. \end{array} \tag{3.3}$$

Here $\boldsymbol{\alpha}$ represents a suitable positive definite and symmetric tensor, while $\mathbf{f}_1$ and $\mathbf{f}_2$ are assigned external forces. When

$$\boldsymbol{\alpha}=\frac{\boldsymbol{\kappa}}{\mu}\quad\text{and}\quad \mathbf{f}_2=-\nabla(\rho g(z-z_0)),$$

equation $(3.3)_1$ is in fact (2.7).

The unknown controls $\boldsymbol{\lambda}_1$ and λ_2 can be obtained by minimizing a suitable cost functional that measures the gap between the velocities $\mathbf{u}_1=\mathbf{u}_1(\boldsymbol{\lambda}_1)$, $\mathbf{u}_2=\mathbf{u}_2(\lambda_2)$ and the pressures $p_1=p_1(\boldsymbol{\lambda}_1)$, $p_2=p_2(\lambda_2)$ on the interfaces Γ_1 and Γ_2, respectively, in a suitable norm. More precisely,

$$(\boldsymbol{\lambda}_1,\lambda_2)=\underset{(\boldsymbol{\mu}_1,\mu_2)}{\operatorname{argmin}}\left[J(\boldsymbol{\mu}_1,\mu_2)=\frac{1}{2}\|\mathbf{u}_1(\boldsymbol{\mu}_1)-\mathbf{u}_2(\mu_2)\|^2_{\Gamma_1}+\frac{1}{2}\|p_2(\mu_2)-p_1(\boldsymbol{\mu}_1)\|^2_{\Gamma_2}\right]. \tag{3.4}$$

For the time being, this expression is a formal one. We will better precise the meaning of J after the discretization of (3.2)–(3.3).

Problem (3.2)–(3.4) is in fact an optimal control problem, in which $(\mathbf{u}_i,p_i)$ (for $i=1,2$) represent the state variables. The solutions of (3.2)–(3.3) in fact depend on both the controls, the right hand side of the momentum equation and the boundary data, but we omit here such dependences for sake of notation.

REMARK 3.1. *Notice that when $inf J=0$, the solution of the optimal control problem (3.2)–(3.4) features the continuity of the velocity field on the interface Γ_1 and the continuity of the pressure on Γ_2, i.e.*

$$\mathbf{u}_1=\mathbf{u}_2 \text{ on } \Gamma_1,\quad p_1=p_2 \text{ on } \Gamma_2.$$

We consider now the weak form of differential subproblems (3.2) and (3.3). We introduce the functional spaces

$$\begin{array}{l} H(\mathrm{div},\Omega)=\{\mathbf{v}\in[L^2(\Omega)]^d:\ \nabla\cdot\mathbf{v}\in L^2(\Omega)\},\\ \mathbf{V}_1=\{\mathbf{v}_1\in[H^1(\Omega_1)]^d:\ \mathbf{v}_1|_{\partial\Omega_1^D}=\mathbf{0}\},\qquad Q_1=L^2(\Omega_1),\\ \mathbf{V}_1^0=\{\mathbf{v}_1\in[H^1(\Omega_1)]^d:\ \mathbf{v}_1|_{(\partial\Omega_1^D\cup\Gamma_1)}=\mathbf{0}\},\\ \mathbf{V}_2=\{\mathbf{v}_2\in H(\mathrm{div},\Omega_2):\mathbf{v}_2\cdot\mathbf{n}_2=0 \text{ on } \partial\Omega_2^N\},\qquad Q_2=L^2(\Omega),\\ \boldsymbol{\Lambda}_1=\{\boldsymbol{\lambda}_1\in[H^{1/2}(\Gamma_1)]^d:\ \exists\mathbf{v}_1\in\mathbf{V}_1:\ \mathbf{v}_1|_{\Gamma_1}=\boldsymbol{\lambda}_1\},\\ \Lambda_2=H^{1/2}(\Gamma_2) \end{array} \tag{3.5}$$

as well as the extension operator $E_1 : \mathbf{\Lambda}_1 \to \mathbf{V}_1$ s.t. $E_1\boldsymbol{\lambda}_1 = \boldsymbol{\lambda}_1$ on Γ_1.

The weak form of system (3.2)–(3.3) reads as follows.
Given $\mathbf{f}_1 \in [L^2(\Omega_1)]^d$, $\mathbf{f}_2 \in H(\mathrm{div}, \Omega_2)$, and $\boldsymbol{\lambda}_1 \in \mathbf{\Lambda}_1$, $\lambda_2 \in \Lambda_2$, we look for $(\mathbf{u}_{1,0}, p_1) \in \mathbf{V}_1^0 \times Q_1$ and $(\mathbf{u}_2, p_2) \in \mathbf{V}_2 \times Q_2$ such that

$$\begin{aligned} &a_1(\mathbf{u}_{1,0}, \mathbf{v}_1) + b_1(\mathbf{v}_1, p_1) = \mathcal{F}_1(\mathbf{v}_1) - a_1(E_1\boldsymbol{\lambda}_1, \mathbf{v}_1) && \forall \mathbf{v}_1 \in \mathbf{V}_1^0 \\ &b_1(\mathbf{u}_{1,0}, q_1) = -b_1(E_1\boldsymbol{\lambda}_1, q_1) && \forall q_1 \in Q_1 \\ &\mathbf{u}_1 = \mathbf{u}_{1,0} + E_1\boldsymbol{\lambda}_1, \end{aligned} \tag{3.6}$$

$$\begin{aligned} &a_2(\mathbf{u}_2, \mathbf{v}_2) + b_2(\mathbf{v}_2, p_2) = \mathcal{F}_2(\mathbf{v}_2) - \langle \mathbf{v}_2 \cdot \mathbf{n}_2, \lambda_2 \rangle_{\Gamma_2} && \forall \mathbf{v}_2 \in \mathbf{V}_2 \\ &b_2(\mathbf{u}_2, q_2) = 0 && \forall q_2 \in Q_2. \end{aligned} \tag{3.7}$$

where:

$$\begin{aligned} &a_1 : \mathbf{V}_1 \times \mathbf{V}_1 \to \mathbb{R}, \quad a_1(\mathbf{u}_1, \mathbf{v}_1) = \int_{\Omega_1} \mu(\nabla \mathbf{u}_1 + \nabla \mathbf{u}_1^T) : \nabla \mathbf{v}_1 d\Omega + \alpha \int_{\Omega_1} \mathbf{u}_1 \cdot \mathbf{v}_1 d\Omega, \\ &b_1 : \mathbf{V}_1 \times Q_1 \to \mathbb{R}, \quad b_1(\mathbf{v}_1, q_1) = -\int_{\Omega_1} q_1 \nabla \cdot \mathbf{v}_1 d\Omega \\ &a_2 : \mathbf{V}_2 \times \mathbf{V}_2 \to \mathbb{R}, \quad a_2(\mathbf{u}_2, \mathbf{v}_2) = \int_{\Omega_2} (\boldsymbol{\alpha}^{-1}\mathbf{u}_2) \cdot \mathbf{v}_2 d\Omega \\ &b_2 : \mathbf{V}_2 \times Q_2 \to \mathbb{R}, \quad b_2(\mathbf{v}_2, q_2) = -\int_{\Omega_2} q_2 \nabla \cdot \mathbf{v}_2 d\Omega, \\ &\mathcal{F}_i : \mathbf{V}_i \to \mathbb{R}, \qquad \mathcal{F}_i(\mathbf{v}_i) = \int_{\Omega_i} \mathbf{f}_i \cdot \mathbf{v}_i d\Omega, \quad i = 1, 2, \end{aligned} \tag{3.8}$$

while $\langle \cdot, \cdot \rangle_{\Gamma_2}$ denotes the duality between $H^{1/2}(\Gamma_2)$ and its dual space.

Problems (3.6)–(3.7) are individually well-posed (see, e.g., [44]); in the next Section we will write their discrete counterpart. We notice that p_2 has a better regularity than merely $L^2(\Omega_2)$, more precisely it belongs to $H^1(\Omega_2)$ (see [44]).

4. *hp*-FEM discretization. For $i = 1, 2$, let $\mathcal{T}_i$ be a partition of the computational domain $\Omega_i \subset \mathbb{R}^d$ in either simplexes or quadrilaterals/hexahedra (quadrilaterals when $d = 2$ and hexahedra when $d = 3$). We denote by $\hat{T}$ the reference element, that can be either the reference simplex with vertexes $\mathbf{0}$ and the points on the axis whose distance from the origin is 1, or the $d-$dimensional cube $(-1, 1)^d$.

We name *simplicial* the partitions composed by simplexes and *quad* those partitions formed by quadrilaterals/hexahedra. The first ones are typical of classical FEM, the others of Spectral Elements Methods (SEM) with tensorial structure (see [7, 8]), from now on we group them under $hp-$FEM.

We suppose that each element $T \in \mathcal{T}_i$ is obtained by a C^1 diffeomorphism $\mathbf{F}_T$ of the reference element $\hat{T}$ and we suppose that two adjacent elements of $\mathcal{T}_i$ share a common vertex, a complete edge, or a complete face (when $d = 3$). For each $T \in \mathcal{T}_i$ we denote by $h_T = \mathrm{diam}(T) = \max_{\mathbf{x},\mathbf{y} \in T} |\mathbf{x} - \mathbf{y}|$ the diameter of element T and we define $h_i = \max_{T \in \mathcal{T}_i} h_T$. Then, when simplicial partitions are considered, we require that the grid is regular in each Ω_i (see, e.g., [44]).

We assume that the meshes $\mathcal{T}_1$ and $\mathcal{T}_2$ match on $\overline{\Omega}_{12}$ so that the interfaces Γ_1 and Γ_2 do not cut any element of the overlapping subdomains Ω_2 and Ω_1, respectively.

Given an integer $p \geq 1$, let us denote by $\mathbb{P}_p$ the space of polynomials whose global degree is less than or equal to p in the variables $x_1, \ldots, x_d$ and by $\mathbb{Q}_p$ the space of

polynomials that are of degree less than or equal to p with respect to each variable $x_1, \ldots, x_d$. The space $\mathbb{P}_p$ is associated with simplicial partitions, while $\mathbb{Q}_p$ to quad ones. We introduce the following finite dimensional spaces in $\overline{\Omega}_i$:

$$X^p_{i,h} = \{v \in C^0(\overline{\Omega}_i) \,:\, v_{|T} \in \mathbb{P}_p,\ \forall T \in \mathcal{T}_i\} \tag{4.1}$$

in the simplicial case and

$$X^p_{i,h} = \{v \in C^0(\overline{\Omega}_i) \,:\, v_{|T} \circ \mathbf{F}_T \in \mathbb{Q}_p,\ \forall T \in \mathcal{T}_i\}, \tag{4.2}$$

for quads. Finally, let $\mathcal{M}_i$ be the set of the nodes $\mathbf{x}_j$ of the mesh $\mathcal{T}_i$.

In the Stokes subdomain we consider either inf-sup stable finite dimensional spaces or stabilized couples of spaces (see, e.g., [4, 23, 25, 30, 43]). In the Darcy subdomain we can either consider stabilized finite dimensional spaces (see, e.g., [39]) to approximate the velocity and the pressure, or adopt a Stokes-compatible formulation as that introduced in [13]. We assume that the polynomials used for the pressure are continuous (see, e.g., [26, 44]). Then, the finite dimensional spaces for velocity and pressure are, respectively,

$$\begin{array}{ll} \mathbf{V}_{1,h} = \mathbf{V}_1 \cap [X^p_{1,h}]^d, & Q_{1,h} = Q_1 \cap X^r_{1,h}, \\ \mathbf{V}^0_{1,h} = \mathbf{V}^0_1 \cap [X^p_{1,h}]^d, & \end{array} \tag{4.3}$$

and

$$\mathbf{V}_{2,h} = \mathbf{V}_2 \cap [X^t_{2,h}]^d, \qquad Q_{2,h} = Q_2 \cap X^s_{2,h}, \tag{4.4}$$

for suitable polynomial degrees p, r, t and s.

Finally, the spaces of discrete Dirichlet controls are defined as

$$\mathbf{\Lambda}_{1,h} = \{\boldsymbol{\lambda}_{1,h} \in [C^0(\overline{\Gamma}_1)]^d :\ \exists \mathbf{v}_{1,h} \in \mathbf{V}_{1,h} \text{ with } \boldsymbol{\lambda}_{1,h} = \mathbf{v}_{1,h}|_{\Gamma_1}\} \tag{4.5}$$

$$\Lambda_{2,h} = \{\lambda_{2,h} \in C^0(\overline{\Gamma}_2) :\ \exists q_{2,h} \in Q_{2,h} \text{ with } \lambda_{2,h} = q_{2,h}|_{\Gamma_2}\}. \tag{4.6}$$

We denote by $N^{\mathbf{u}}_{\Omega_1}$, $N^p_{\Omega_1}$, N_{Γ_1}, $N^{\mathbf{u}}_{\Omega_2}$, $N^p_{\Omega_2}$, and N_{Γ_2} the cardinality of $\mathbf{V}^0_{1,h}$, $Q_{1,h}$, $\mathbf{\Lambda}_{1,h}$, $\mathbf{V}_{2,h}$, $Q_{2,h}$, and $\Lambda_{2,h}$, respectively.

In each discrete functional space we consider the basis of the characteristic Lagrange polynomials associated with the nodes of $\mathcal{M}_i$ and we denote by $\boldsymbol{\varphi}_{i,\ell}$ (for $i = 1, 2$ and $\ell = 1, \ldots, N^{\mathbf{u}}_{\Omega_i}$) and $\psi_{i,\ell}$ (for $i = 1, 2$ and $\ell = 1, \ldots, N^p_{\Omega_i}$) the basis functions of $\mathbf{V}^0_{1,h}$, $\mathbf{V}_{2,h}$ and $Q_{1,h}$, $Q_{2,h}$ respectively.

The basis functions in $\mathbf{\Lambda}_{1,h}$ are denoted by $\boldsymbol{\eta}_{1,\ell}$ (for $\ell = 1, \ldots, N_{\Gamma_1}$) and they are defined by restriction to Γ_1 of the basis functions of $\mathbf{V}_{1,h}$ that are not identically null on Γ_1. Similarly we define the basis function $\eta_{2,\ell}$ (for $\ell = 1, \ldots, N_{\Gamma_2}$) of $\Lambda_{2,h}$, starting from the basis in $Q_{2,h}$.

Because of the difficulty to compute integrals exactly for large p, typically when quad partitions are used, Legendre-Gauss-Lobatto quadrature formulas are used to approximate both the bilinear forms $\mathcal{A}_i$ and the L^2-inner products in Ω_i (as well as on the interfaces). This leads to the so called *Galerkin approach with Numerical Integration* (G-NI) [7, 6] and to the Spectral Element Method with Numerical Integration (SEM-NI).

We define the discrete counterpart of the extension operator: $E_{1,h} : \mathbf{\Lambda}_{1,h} \to \mathbf{V}_{1,h}$ s.t. $E_{1,h}\boldsymbol{\lambda}_{1,h} = \boldsymbol{\lambda}_{1,h}$ on Γ_1 and $(E_{1,h}\boldsymbol{\lambda}_{1,h})(\mathbf{x}_j) = \mathbf{0}$ for any $\mathbf{x}_j \in \mathcal{M}_1 \cap (\overline{\Omega}_1 \setminus (\Gamma_1 \cup \partial\Omega_1^N))$.

The discrete counterpart of (3.6)–(3.7) reads: given $\mathbf{f}_1 \in [L^2(\Omega_1)]^d$, $\mathbf{f}_2 \in H(\mathrm{div}, \Omega_2)$, given $\boldsymbol{\lambda}_{1,h} \in \boldsymbol{\Lambda}_{1,h}$, $\lambda_{2,h} \in \Lambda_{2,h}$ we look for $(\mathbf{u}_{1,0,h}, p_{1,h}) \in \mathbf{V}^0_{1,h} \times Q_{1,h}$ and $(\mathbf{u}_{2,h}, p_{2,h}) \in \mathbf{V}_{2,h} \times Q_{2,h}$ such that

$$\begin{aligned}
&\mathcal{A}_{1,h}(\mathbf{u}_{1,0,h}, p_{1,h}; \mathbf{v}_{1,h}, q_{1,h}) = -\mathcal{B}_{1,h}(E_{1,h}\boldsymbol{\lambda}_{1,h}; \mathbf{v}_{1,h}, q_{1,h}) + \mathcal{F}_{1,h}(\mathbf{v}_{1,h}, q_{1,h}) \\
&\qquad\qquad \forall (\mathbf{v}_{1,h}, q_{1,h}) \in \mathbf{V}^0_{1,h} \times Q_{1,h} \\
&\mathbf{u}_{1,h} = \mathbf{u}_{1,0,h} + E_{1,h}\boldsymbol{\lambda}_{1,h} \\
&\mathcal{A}_{2,h}(\mathbf{u}_{2,h}, p_{2,h}; \mathbf{v}_{2,h}, q_{2,h}) = -\mathcal{B}_{2,h}(\lambda_{2,h}; \mathbf{v}_{2,h}) + \mathcal{F}_{2,h}(\mathbf{v}_{2,h}, q_{2,h}) \\
&\qquad\qquad \forall (\mathbf{v}_{2,h}, q_{2,h}) \in \mathbf{V}_{2,h} \times Q_{2,h}
\end{aligned} \tag{4.7}$$

where, chosen $\gamma_1 \in \{-1, 0, 1\}$, and being $\tau_k = \tau_k(\mathbf{x})$ a suitable stabilization parameter depending on both mesh size h and local polynomial degree (see, e.g. [23, 25]), we set:

$$\begin{aligned}
&\mathcal{A}_{1,h}(\mathbf{w}_{1,h}, s_{1,h}; \mathbf{v}_{1,h}, q_{1,h}) = a_1(\mathbf{w}_{1,h}, \mathbf{v}_{1,h}) + b_1(\mathbf{v}_{1,h}, s_{1,h}) - b_1(\mathbf{w}_{1,h}, q_{1,h}) \\
&\qquad + \sum_{T_k \in \mathcal{T}_1} (-\nu\Delta\mathbf{w}_{1,h} + \nabla s_{1,h} + \alpha\mathbf{w}_{1,h}, \tau_k(\gamma_1\nu\Delta\mathbf{v}_{1,h} + \nabla q_{1,h} + \alpha\mathbf{v}_{1,h}))_{L^2(T_k)} \\
&\mathcal{B}_{1,h}(\mathbf{w}_{1,h}; \mathbf{v}_{1,h}, q_{1,h}) = \mathcal{A}_{1,h}(\mathbf{w}_{1,h}, 0; \mathbf{v}_{1,h}, q_{1,h}) \\
&\mathcal{F}_{1,h}(\mathbf{v}_{1,h}, q_{1,h}) = \mathcal{F}_1(\mathbf{v}_{1,h}) + \sum_{T_k \in \mathcal{T}_1} (\mathbf{f}_1, \tau_k(\gamma_1\nu\Delta\mathbf{v}_{1,h} + \nabla q_{1,h} + \alpha\mathbf{v}_{1,h}))_{L^2(T_k)}.
\end{aligned} \tag{4.8}$$

Moreover,

$$\begin{aligned}
&\mathcal{A}_{2,h}(\mathbf{w}_{2,h}, s_{2,h}; \mathbf{v}_{2,h}, q_{2,h}) = a_2(\mathbf{w}_{2,h}, \mathbf{v}_{2,h}) + b_2(\mathbf{v}_{2,h}, s_{2,h}) - b_2(\mathbf{w}_{2,h}, q_{2,h}) \\
&\qquad +\gamma_{2,1}(\boldsymbol{\alpha}^{-1}\mathbf{w}_{2,h} + \nabla s_{2,h}, \boldsymbol{\alpha}/2(-\boldsymbol{\alpha}^{-1}\mathbf{v}_{2,h} + \nabla q_{2,h}))_{L^2(\Omega_2)} \\
&\qquad +\gamma_{2,2}(\nabla \cdot \mathbf{w}_{2,h}, \|\boldsymbol{\alpha}^{-1}\|\nabla \cdot \mathbf{v}_{2,h})_{L^2(\Omega_2)} \\
&\qquad +\gamma_{2,3}(\boldsymbol{\alpha}\nabla \times (\boldsymbol{\alpha}^{-1}\mathbf{w}_{2,h}), \nabla \times (\boldsymbol{\alpha}^{-1}\mathbf{v}_{2,h}))_{L^2(\Omega_2)}, \\
&\mathcal{B}_{2,h}(s_{2,h}; \mathbf{v}_{2,h}) = \langle \mathbf{v}_{2,h} \cdot \mathbf{n}_2, s_{2,h} \rangle_{\Gamma_2} \\
&\mathcal{F}_{2,h}(\mathbf{v}_{2,h}, q_{2,h}) = \mathcal{F}_2(\mathbf{v}_{2,h}) + \gamma_{2,1}(\mathbf{f}_2, \boldsymbol{\alpha}/2(-\boldsymbol{\alpha}^{-1}\mathbf{v}_{2,h} + \nabla q_{2,h}))_{L^2(\Omega_2)} \\
&\qquad +\gamma_{2,3}(\boldsymbol{\alpha}\nabla \times (\boldsymbol{\alpha}^{-1}\mathbf{f}_2), \nabla \times (\boldsymbol{\alpha}^{-1}\mathbf{v}_{2,h}))_{L^2(\Omega_2)},
\end{aligned} \tag{4.9}$$

where $\gamma_{2,1} = 1$, $\gamma_{2,2} = h^2/2$, $\gamma_{2,3} = 0$ if the stabilization method [39] is used, while $\gamma_{2,1} = 0$ and $\gamma_{2,2}$ and $\gamma_{2,3}$ are suitably chosen parameters if the formulation proposed in [13] is adopted.

Notice that setting $\tau_k = 0$ in (4.8), we recover the classical weak form of the Stokes problem, that is well posed once the discrete spaces satisfy the inf-sup condition ([4]).

We make the following remarks. In view of the choice done for the space $\Lambda_{2,h}$, the trace of $p_{2,h}$ on Γ_2 belongs to $H^{1/2}(\Gamma_2)$. Moreover, by definition of the space $Q_{1,h}$ (also Darcy pressures are chosen continuous) it holds $Q_{1,h} \subset H^1(\Omega_1)$, thus the trace of $p_{1,h}$ on Γ_2 is well defined and it belongs to $H^{1/2}(\Gamma_2)$. Therefore, the L^2 norm of the gap $(p_{2,h} - p_{1,h})$ on Γ_2 is finite.

The same arguments can be applied to conclude that the traces of both $\mathbf{u}_{1,h}$ and $\mathbf{u}_{2,h}$ on Γ_1 belongs to $[H^{1/2}(\Gamma_1)]^d$ so that $\|\mathbf{u}_{1,h} - \mathbf{u}_{2,h}\|_{L^2(\Gamma_1)}$ is meaningful.

We now replace the minimization problem (3.4) by its approximate version:

$$\begin{aligned}(\boldsymbol{\lambda}_{1,h},\lambda_{2,h}) &= \underset{(\boldsymbol{\mu}_{1,h},\mu_{2,h})}{\operatorname{argmin}} \Big[J(\boldsymbol{\mu}_{1,h},\mu_{2,h}) \\ &= \frac{1}{2}\|\mathbf{u}_{1,h}(\boldsymbol{\mu}_{1,h})-\mathbf{u}_{2,h}(\mu_{2,h})\|^2_{L^2(\Gamma_1)}+\frac{1}{2}\|p_{2,h}(\mu_{2,h})-p_{1,h}(\boldsymbol{\mu}_{1,h})\|^2_{L^2(\Gamma_2)}\Big].\end{aligned} \tag{4.10}$$

REMARK 4.1. *The use of L^2-norm instead of $H^{1/2}-$norm is justified because it is cheaper to compute.*

5. Analysis of ICDD method. In this Section we analyse the well-posedness of the optimal control problem (4.7)– (4.10).

Given $\boldsymbol{\lambda}_h=(\boldsymbol{\lambda}_{1,h},\lambda_{2,h})$, and the known functions $\mathbf{f}_i$ $(i=1,2)$, let us explicitely express the dependence of the solutions $(\mathbf{u}_{i,h},p_{i,h})$ of (4.7) on both the data $\mathbf{f}=\{\mathbf{f}_1,\mathbf{f}_2\}$ and the control $\boldsymbol{\lambda}_h$ by writing $\mathbf{u}_{i,h}=\mathbf{u}_{i,h}^{\boldsymbol{\lambda}_h,\mathbf{f}}$ and $p_{i,h}=p_{i,h}^{\boldsymbol{\lambda}_h,\mathbf{f}}$. When $\mathbf{f}_i=\mathbf{0}$, we simplify this notation by writing $\mathbf{u}_{i,h}^{\boldsymbol{\lambda}_h}=\mathbf{u}_{i,h}^{\boldsymbol{\lambda}_h,\mathbf{0}}$ and $p_{i,h}^{\boldsymbol{\lambda}_h}=p_{i,h}^{\boldsymbol{\lambda}_h,\mathbf{0}}$.

Let us define $\boldsymbol{\Lambda}_h=\boldsymbol{\Lambda}_{1,h}\times\Lambda_{2,h}$ and

$$|\!|\!|\boldsymbol{\lambda}_h|\!|\!| = \Big(\|\mathbf{u}_{1,h}^{\boldsymbol{\lambda}_h}-\mathbf{u}_{2,h}^{\boldsymbol{\lambda}_h}\|^2_{L^2(\Gamma_1)}+\|p_{2,h}^{\boldsymbol{\lambda}_h}-p_{1,h}^{\boldsymbol{\lambda}_h}\|^2_{L^2(\Gamma_2)}\Big)^{1/2},\quad \forall\boldsymbol{\lambda}_h\in\boldsymbol{\Lambda}_h. \tag{5.1}$$

LEMMA 5.1. *$|\!|\!|\boldsymbol{\lambda}_h|\!|\!|$ is a norm on the control space $\boldsymbol{\Lambda}_h$.*

Proof. $|\!|\!|\cdot|\!|\!|$ is obviously a seminorm, therefore we limit ourselves to show that $|\!|\!|\boldsymbol{\lambda}_h|\!|\!|=0$ implies $\boldsymbol{\lambda}_h=\mathbf{0}$.

We observe that $|\!|\!|\boldsymbol{\lambda}_h|\!|\!|=0$ if and only if the solution of (4.7) satisfies

$$\boldsymbol{\lambda}_{1,h}=\mathbf{u}_{1,h}^{\boldsymbol{\lambda}_h}=\mathbf{u}_{2,h}^{\boldsymbol{\lambda}_h}\text{ on }\Gamma_1\text{ and }\lambda_{2,h}=p_{2,h}^{\boldsymbol{\lambda}_h}=p_{1,h}^{\boldsymbol{\lambda}_h}\text{ on }\Gamma_2,$$

that is, if and only if it holds

$$\begin{aligned}
&\mathcal{A}_{1,h}(\mathbf{u}_{1,0,h}^{\boldsymbol{\lambda}_h},p_{1,h}^{\boldsymbol{\lambda}_h};\mathbf{v}_{1,h},q_{1,h})=-\mathcal{B}_{1,h}(E_{1,h}(\boldsymbol{\lambda}_{1,h});\mathbf{v}_{1,h},q_{1,h}) \quad \forall(\mathbf{v}_{1,h},q_{1,h})\in\mathbf{V}^0_{1,h}\times Q_{1,h}\\
&\mathbf{u}_{1,h}^{\boldsymbol{\lambda}_h}=\mathbf{u}_{1,0,h}^{\boldsymbol{\lambda}_h}+E_{1,h}(\boldsymbol{\lambda}_{1,h})\\
&\boldsymbol{\lambda}_{1,h}=\mathbf{u}_{2,h}^{\boldsymbol{\lambda}_h}|_{\Gamma_1}\\
&\mathcal{A}_{2,h}(\mathbf{u}_{2,h}^{\boldsymbol{\lambda}_h},p_{2,h}^{\boldsymbol{\lambda}_h};\mathbf{v}_{2,h},q_{2,h})=-\mathcal{B}_{2,h}(\lambda_{2,h};\mathbf{v}_{2,h}) \quad \forall(\mathbf{v}_{2,h},q_{2,h})\in\mathbf{V}_{2,h}\times Q_{2,h}\\
&\lambda_{2,h}=p_{1,h}^{\boldsymbol{\lambda}_h}|_{\Gamma_2}.
\end{aligned} \tag{5.2}$$

The algebraic counterpart of (5.2) reads

$$\underbrace{\left[\begin{array}{cc|cc} A_{11} & A_{1\Gamma_1} & 0 & 0\\ 0 & I & -R_{12} & 0\\ \hline 0 & 0 & A_{22} & A_{2\Gamma_2}\\ -R_{21} & 0 & 0 & I\end{array}\right]}_{G}\left[\begin{array}{c}\underline{\mathbf{U}}_1\\ \underline{\boldsymbol{\lambda}}_1\\ \hline \underline{\mathbf{U}}_2\\ \underline{\boldsymbol{\lambda}}_2\end{array}\right]=\left[\begin{array}{c}\mathbf{0}\\ \mathbf{0}\\ \hline \mathbf{0}\\ \mathbf{0}\end{array}\right], \tag{5.3}$$

where:
- $\underline{\mathbf{U}}_i\in\mathbb{R}^{N_{\Omega_i}}$ contains the degrees of freedom of both velocity and pressure in Ω_i;
- $\underline{\boldsymbol{\lambda}}_i\in\mathbb{R}^{N_{\Gamma_i}}$ contains the degrees of freedom of the control function on Γ_i;
- A_{ii} is the matrix associated with the bilinear form $\mathcal{A}_{i,h}$;
- $A_{i\Gamma_i}$ is the matrix associated with the bilinear form $\mathcal{B}_{i,h}$;

- $R_{ij} \in \mathbb{R}^{N_{\Gamma_i} \times N_{\Omega_i}}$ are matrices of zeros and ones that perform the restriction of $\underline{\mathbf{U}}_j$ (only for the part involving either the velocity degrees of freedom in the Stokes domain or the pressure ones in the Darcy domain) to Γ_i.

We want to prove that $Ker(G) = \{[\mathbf{0}, \mathbf{0}, \mathbf{0}, \mathbf{0}]^T\}$. For that, we will make use of the relations

$$Ker(A) = (Im(A^T))^{\perp}, \tag{5.4}$$

$$Ker\left(\begin{bmatrix} B \\ C \end{bmatrix}\right) = Ker(B) \cap Ker(C), \tag{5.5}$$

that hold for generic rectangular matrices A, B, and C, such that B and C have the same number of columns.

Let us split matrix G in 2×2 blocks G_{ij} $(i, j = 1, 2)$ of size $N_i \times N_j$, as depicted in (5.3). Since the local Stokes and Darcy subproblems are well-posed, blocks G_{ii} are non-singular, moreover we have

$$Im([G_{11}\ G_{12}]^T) = \begin{bmatrix} Im(G_{11}^T) \\ Im(G_{12}^T) \end{bmatrix} = \begin{bmatrix} Im\left(\begin{bmatrix} A_{11}^T & 0 \\ A_{1\Gamma_1}^T & I \end{bmatrix}\right) \\ Im\left(\begin{bmatrix} 0 & -R_{12}^T \\ 0 & 0 \end{bmatrix}\right) \end{bmatrix} = \begin{bmatrix} \mathbb{R}^{N_1} \\ \begin{bmatrix} \mathbb{R}^{N_{\Gamma_1}} \\ \mathbf{0}_{N_2 - N_{\Gamma_1}} \end{bmatrix} \end{bmatrix}$$

and

$$Im([G_{21}\ G_{22}]^T) = \begin{bmatrix} Im(G_{21}^T) \\ Im(G_{22}^T) \end{bmatrix} = \begin{bmatrix} Im\left(\begin{bmatrix} 0 & -R_{21}^T \\ 0 & 0 \end{bmatrix}\right) \\ Im\left(\begin{bmatrix} A_{22}^T & 0 \\ A_{2\Gamma_2}^T & I \end{bmatrix}\right) \end{bmatrix} = \begin{bmatrix} \begin{bmatrix} \mathbb{R}^{N_{\Gamma_2}} \\ \mathbf{0}_{N_1 - N_{\Gamma_2}} \end{bmatrix} \\ \mathbb{R}^{N_2} \end{bmatrix}.$$

Then, thanks to (5.4),

$$Ker([G_{11}\ G_{12}]) = \left(Im([G_{11}\ G_{12}]^T)\right)^{\perp} = \begin{bmatrix} \mathbf{0}_{N_1} \\ \begin{bmatrix} \mathbb{R}^{N_2 - N_{\Gamma_1}} \\ \mathbf{0}_{N_{\Gamma_1}} \end{bmatrix} \end{bmatrix},$$

$$Ker([G_{21}\ G_{22}]) = \left(Im([G_{21}\ G_{22}]^T)\right)^{\perp} = \begin{bmatrix} \begin{bmatrix} \mathbb{R}^{N_1 - N_{\Gamma_2}} \\ \mathbf{0}_{N_{\Gamma_2}} \end{bmatrix} \\ \mathbf{0}_{N_2} \end{bmatrix},$$

and finally, using (5.5),

$$Ker(G) = (Ker([G_{11}\ G_{12}])) \cap (Ker([G_{21}\ G_{22}])) = \{[\mathbf{0}, \mathbf{0}, \mathbf{0}, \mathbf{0}]^T\}. \tag{5.6}$$

This implies, in particular, that $\boldsymbol{\lambda}_{1,h} = \mathbf{0}$ and $\lambda_{2,h} = 0$. □

THEOREM 5.2. *The minimization problem (4.10) (where the state variables satisfy (4.7)), has a unique solution $\boldsymbol{\lambda}_h \in \boldsymbol{\Lambda}_h$ satisfying the Euler-Lagrange equation*

$$\begin{aligned} \langle J'(\boldsymbol{\lambda}_h), \boldsymbol{\eta}_h \rangle = \quad & \int_{\Gamma_1} (\mathbf{u}_{1,h}^{\boldsymbol{\lambda}_h, \mathbf{f}} - \mathbf{u}_{2,h}^{\boldsymbol{\lambda}_h, \mathbf{f}})(\mathbf{u}_{1,h}^{\boldsymbol{\eta}_h} - \mathbf{u}_{2,h}^{\boldsymbol{\eta}_h}) \\ & + \int_{\Gamma_2} (p_{2,h}^{\boldsymbol{\lambda}_h, \mathbf{f}} - p_{1,h}^{\boldsymbol{\lambda}_h, \mathbf{f}})(p_{2,h}^{\boldsymbol{\eta}_h} - p_{1,h}^{\boldsymbol{\eta}_h}) = 0 \qquad \forall \boldsymbol{\eta}_h \in \boldsymbol{\Lambda}_h. \end{aligned} \tag{5.7}$$

Proof. We set

$$\pi(\boldsymbol{\lambda}_h, \boldsymbol{\mu}_h) = \frac{1}{2}(\mathbf{u}_{1,h}^{\boldsymbol{\lambda}_h} - \mathbf{u}_{2,h}^{\boldsymbol{\lambda}_h}, \mathbf{u}_{1,h}^{\boldsymbol{\mu}_h} - \mathbf{u}_{2,h}^{\boldsymbol{\mu}_h})_{L^2(\Gamma_1)} + \frac{1}{2}(p_{2,h}^{\boldsymbol{\lambda}_h} - p_{1,h}^{\boldsymbol{\lambda}_h}, p_{2,h}^{\boldsymbol{\mu}_h} - p_{1,h}^{\boldsymbol{\mu}_h})_{L^2(\Gamma_2)} \tag{5.8}$$

and

$$\mathcal{L}(\boldsymbol{\mu}_h) = -\frac{1}{2}(\mathbf{u}_{1,h}^{0,\mathbf{f}} - \mathbf{u}_{2,h}^{0,\mathbf{f}}, \mathbf{u}_{1,h}^{\boldsymbol{\mu}_h} - \mathbf{u}_{2,h}^{\boldsymbol{\mu}_h})_{L^2(\Gamma_1)} + \frac{1}{2}(p_{2,h}^{0,\mathbf{f}} - p_{1,h}^{0,\mathbf{f}}, p_{2,h}^{\boldsymbol{\mu}_h} - p_{1,h}^{\boldsymbol{\mu}_h})_{L^2(\Gamma_2)}, \quad (5.9)$$

so that

$$J(\boldsymbol{\mu}_h) = \pi(\boldsymbol{\mu}_h, \boldsymbol{\mu}_h) - 2\mathcal{L}(\boldsymbol{\mu}_h) + \frac{1}{2}\|\mathbf{u}_{1,h}^{0,\mathbf{f}} - \mathbf{u}_{2,h}^{0,\mathbf{f}}\|^2_{L^2(\Gamma_1)} + \frac{1}{2}\|p_{2,h}^{0,\mathbf{f}} - p_{1,h}^{0,\mathbf{f}}\|^2_{L^2(\Gamma_2)}. \quad (5.10)$$

Here, $\pi : \boldsymbol{\Lambda}_h \times \boldsymbol{\Lambda}_h \to \mathbb{R}$ is a bilinear symmetric form and thanks to Lemma 5.1 it is continuous and coercive with respect to the norm $|||\cdot|||$, while $\mathcal{L} : \boldsymbol{\Lambda}_h \to \mathbb{R}$ is a linear and continuous functional.

Moreover, $(\boldsymbol{\Lambda}_h, |||\cdot|||)$ is a finite dimensional Hilbert space and, by applying classical results of the calculus of variations, both existence and uniqueness of solution follow. The Euler-Lagrange equation (5.7) follows by noticing that

$$\langle J'(\boldsymbol{\lambda}_h), \boldsymbol{\mu}_h\rangle = 2\pi(\boldsymbol{\lambda}_h, \boldsymbol{\mu}_h) - 2\mathcal{L}(\boldsymbol{\mu}_h) \qquad \forall \boldsymbol{\lambda}_h, \boldsymbol{\mu}_h \in \boldsymbol{\Lambda}_h. \quad (5.11)$$

□

5.1. Optimality system. We associate the following optimality system with the Euler Lagrange equation (5.7). Find the state solutions $(\mathbf{u}_{i,h}^{\boldsymbol{\lambda}_h}, p_{i,h}^{\boldsymbol{\lambda}_h}) \in \mathbf{V}_{i,h} \times Q_{i,h}$, the dual solutions $(\mathbf{w}_{i,h}^{\boldsymbol{\lambda}_h}, q_{i,h}^{\boldsymbol{\lambda}_h}) \in \mathbf{V}_{i,h} \times Q_{i,h}$ and the control variable $\boldsymbol{\lambda}_h = (\boldsymbol{\lambda}_{1,h}, \lambda_{2,h}) \in \boldsymbol{\Lambda}_{1,h} \times \Lambda_{2,h}$ satisfying

State Problems

find $\mathbf{u}_{1,0,h} \in \mathbf{V}_{1,h}^0,\ p_{1,h} \in Q_{1,h}$:

$$\begin{cases} \mathcal{A}_{1,h}(\mathbf{u}_{1,0,h}, p_{1,h}; \mathbf{v}_{1,h}, q_{1,h}) = -\mathcal{B}_{1,h}(E_{1,h}\boldsymbol{\lambda}_{1,h}; \mathbf{v}_{1,h}, q_{1,h}) + \mathcal{F}_{1,h}(\mathbf{v}_{1,h}, q_{1,h}) \\ \qquad\qquad \forall (\mathbf{v}_{1,h}, q_{1,h}) \in \mathbf{V}_{1,h}^0 \times Q_{1,h} \\ \mathbf{u}_{1,h} = \mathbf{u}_{1,0,h} + E_{1,h}\boldsymbol{\lambda}_{1,h}, \end{cases} \quad (5.12)$$

find $\mathbf{u}_{2,h} \in \mathbf{V}_{2,h},\ p_{2,h} \in Q_{2,h}$:

$$\begin{aligned} \mathcal{A}_{2,h}(\mathbf{u}_{2,h}, p_{2,h}; \mathbf{v}_{2,h}, q_{2,h}) &= -\mathcal{B}_{2,h}(\lambda_{2,h}; \mathbf{v}_{2,h}) + \mathcal{F}_{2,h}(\mathbf{v}_{2,h}, q_{2,h}) \\ &\qquad \forall (\mathbf{v}_{2,h}, q_{2,h}) \in \mathbf{V}_{2,h} \times Q_{2,h}; \end{aligned} \quad (5.13)$$

Dual Problems

find $\mathbf{w}_{1,0,h} \in \mathbf{V}_{1,h}^0,\ s_{1,h} \in Q_{1,h}$:

$$\begin{cases} \mathcal{A}_{1,h}(\mathbf{w}_{1,0,h}, s_{1,h}; \mathbf{v}_{1,h}, q_{1,h}) = -\mathcal{B}_{1,h}(E_{1,h}((\mathbf{u}_{1,h} - \mathbf{u}_{2,h})|_{\Gamma_1}); \mathbf{v}_{1,h}, q_{1,h}) \\ \qquad\qquad \forall (\mathbf{v}_{1,h}, q_{1,h}) \in \mathbf{V}_{1,h}^0 \times Q_{1,h} \\ \mathbf{u}_{1,h} = \mathbf{u}_{1,0,h} + E_{1,h}(\mathbf{u}_{1,h} - \mathbf{u}_{2,h}), \end{cases} \quad (5.14)$$

find $\mathbf{w}_{2,h} \in \mathbf{V}_{2,h},\ s_{2,h} \in Q_{2,h}$:

$$\begin{aligned} \mathcal{A}_{2,h}(\mathbf{w}_{2,h}, s_{2,h}; \mathbf{v}_{2,h}, q_{2,h}) &= -\mathcal{B}_{2,h}((p_{2,h} - p_{1,h})|_{\Gamma_2}; \mathbf{v}_{2,h}) \\ &\qquad \forall (\mathbf{v}_{2,h}, q_{2,h}) \in \mathbf{V}_{2,h} \times Q_{2,h}; \end{aligned} \quad (5.15)$$

Interface Equations

$$\begin{aligned} &\int_{\Gamma_1} (\mathbf{u}_{1,h} - \mathbf{u}_{2,h} + \mathbf{w}_{2,h})\boldsymbol{\eta}_{1,h} = 0, \quad \forall \boldsymbol{\eta}_{1,h} \in \boldsymbol{\Lambda}_{1,h} \\ &\int_{\Gamma_2} (p_{2,h} - p_{1,h} + s_{1,h})\eta_{2,h} = 0, \qquad \forall \eta_{2,h} \in \Lambda_{2,h}. \end{aligned} \quad (5.16)$$

Note that the solutions $\mathbf{u}_{i,h}$, $p_{i,h}$ are in fact $\mathbf{u}_{i,h}^{\boldsymbol{\lambda}_h}$, $p_{i,h}^{\boldsymbol{\lambda}_h}$, respectively.

THEOREM 5.3. *The system (5.12)–(5.16) has a unique solution whose control component $\boldsymbol{\lambda}_h = (\boldsymbol{\lambda}_{1,h}, \lambda_{2,h})$ is the solution of (4.10) (or equivalently (5.7)), with constraints (4.7).*

Proof. Existence. Let $\boldsymbol{\lambda}_h$ be the solution of (5.7), then: $\mathbf{u}_{1,h}^{\boldsymbol{\lambda}_h,\mathbf{f}} - \mathbf{u}_{2,h}^{\boldsymbol{\lambda}_h,\mathbf{f}} = \mathbf{0}$ on Γ_1 and $p_{2,h}^{\boldsymbol{\lambda}_h,\mathbf{f}} - p_{1,h}^{\boldsymbol{\lambda}_h,\mathbf{f}} = 0$ on Γ_2, (5.12)–(5.13) are satisfied with $\mathbf{u}_{i,h} = \mathbf{u}_{i,h}^{\boldsymbol{\lambda}_h}$, $p_{i,h} = p_{i,h}^{\boldsymbol{\lambda}_h}$, and the solutions $(\mathbf{w}_{i,h}, s_{i,h})$ of the dual problems (5.14)–(5.15) are null in $\overline{\Omega}_i$. Therefore, equations (5.16) are satisfied and (5.12)–(5.16) admits at least one solution.

Uniqueness. In view of the linearity of both Stokes and Darcy equations, it suffices to prove that if $\mathbf{f}_1 = \mathbf{0}$, $\mathbf{f}_2 = \mathbf{0}$, then the solution of (5.12)–(5.16) is the null one. From (5.16) it follows that $\mathbf{w}_{2,h} = -(\mathbf{u}_{1,h} - \mathbf{u}_{2,h})$ on Γ_1 and $s_{1,h} = -(p_{2,h} - p_{1,h})$ on Γ_2, therefore (5.14)–(5.15) becomes

$$\begin{aligned}
&\mathcal{A}_{1,h}(\mathbf{w}_{1,0,h}, s_{1,h}; \mathbf{v}_{1,h}, q_{1,h}) = -\mathcal{B}_{1,h}(E_{1,h}(-\mathbf{w}_{2,h}^{\boldsymbol{\lambda}_h}|_{\Gamma_1}); \mathbf{v}_{1,h}, q_{1,h}) \\
&\qquad\qquad \forall (\mathbf{v}_{1,h}, q_{1,h}) \in \mathbf{V}_{1,h}^0 \times Q_{1,h} \\
&\mathbf{w}_{1,h} = \mathbf{w}_{1,0,h} + E_{1,h}(\mathbf{w}_{2,h}^{\boldsymbol{\lambda}_h}|_{\Gamma_1}) \\
&\mathcal{A}_{2,h}(\mathbf{w}_{2,h}, s_{2,h}; \mathbf{v}_{2,h}, q_{2,h}) = -\mathcal{B}_{2,h}(-s_{1,h}^{\boldsymbol{\lambda}_h}; \mathbf{v}_{2,h}) \\
&\qquad\qquad \forall (\mathbf{v}_{2,h}, q_{2,h}) \in \mathbf{V}_{2,h} \times Q_{2,h}
\end{aligned}$$

By the same arguments used in the proof of Lemma (5.1), it follows that $\mathbf{w}_{i,h} = \mathbf{0}$ and $s_{i,h} = 0$ in $\overline{\Omega}_i$, for $= 1, 2$. Then, by (5.16), we have $\mathbf{u}_{1,h} = \mathbf{u}_{2,h}$ on Γ_1 and $p_{1,h} = p_{2,h}$ on Γ_2. Again proceeding as before, it follows $\mathbf{u}_{i,h} = \mathbf{0}$ and $p_{i,h} = 0$ in $\overline{\Omega}_i$, and then $\boldsymbol{\lambda}_1 = \mathbf{0}$ and $\lambda_2 = 0$. □

5.2. Algebraic formulation of the optimality system. In this section we derive the algebraic form of the optimality system, then we propose an efficient algorithm for its solution.

The Optimality System (OS) (5.12)–(5.16) has ten unknown functions:
- the primal state variables $\mathbf{u}_{i,h}$ and $p_{i,h}$, for $i = 1, 2$,
- the dual state variables $\mathbf{w}_{i,h}$ and $s_{i,h}$, for $i = 1, 2$,
- the control variables $\boldsymbol{\lambda}_{1,h}, \lambda_{2,h}$.

Let us introduce the following arrays:

$$\begin{aligned}
&\underline{\mathbf{u}}_1 = [\mathbf{u}_{1,h}^0(\mathbf{x}_j)], \quad \underline{p}_1 = [p_{1,h}(\mathbf{x}_j)], \quad \underline{\mathbf{w}}_1 = [\mathbf{w}_{1,h}^0(\mathbf{x}_j)], \quad \underline{s}_1 = [s_{1,h}(\mathbf{x}_j)], \\
&\underline{\mathbf{u}}_2 = [\mathbf{u}_{2,h}(\mathbf{x}_j)], \quad \underline{p}_2 = [p_{2,h}(\mathbf{x}_j)], \quad \underline{\mathbf{w}}_2 = [\mathbf{w}_{2,h}(\mathbf{x}_j)], \quad \underline{s}_2 = [s_{2,h}(\mathbf{x}_j)],
\end{aligned}$$

$$\underline{\boldsymbol{\lambda}}_1 = [\boldsymbol{\lambda}_{1,h}(\mathbf{x}_j)], \text{ with } \mathbf{x}_j \in \Gamma_1, \quad \underline{\lambda}_2 = [\lambda_{2,h}(\mathbf{x}_j)], \text{ with } \mathbf{x}_j \in \Gamma_2,$$

$$\begin{aligned}
&\mathsf{A}_i = [(a_i)_{\ell,j}] = [\mathcal{A}_{i,h}(\boldsymbol{\varphi}_{i,j}, \psi_{i,j}; \boldsymbol{\varphi}_{i,\ell}, \psi_{i,\ell})], \quad \underline{\mathbf{f}}_1 = [\mathcal{F}_{i,h}(\boldsymbol{\varphi}_{i,\ell}, \psi_{i,\ell})], \\
&\mathsf{B}_1 = [(b_1)_{\ell,j}] = [\mathcal{B}_{1,h}(E_{1,h}\boldsymbol{\eta}_{1,j}; \boldsymbol{\varphi}_{1,\ell}, \psi_{1,\ell})], \quad \mathsf{B}_2 = [(b_2)_{\ell,j}] = [\mathcal{B}_{2,h}(\eta_{2,j}; \boldsymbol{\varphi}_{2,\ell})].
\end{aligned}$$

We then define:
- T_{ij}, the matrix implementing the interpolation on Γ_i of a scalar function defined in Ω_j,

- $\mathsf{M}_i^{\Gamma_i}$, the $(d-1)$-dimensional mass matrix associated with the interface Γ_i,
- their d-block versions $\mathbf{T}_{ij} = diag(\underbrace{\mathsf{T}_{ij}, \ldots, \mathsf{T}_{ij}}_{d})$, $\mathbf{M}_i^{\Gamma_i} = diag(\underbrace{\mathsf{M}_i^{\Gamma_i}, \ldots, \mathsf{M}_i^{\Gamma_i}}_{d})$,

and set

$$\widetilde{\mathsf{T}}_{12} = \begin{bmatrix} \mathbf{T}_{12} & 0 \\ 0 & 0 \end{bmatrix}, \qquad \widetilde{\mathsf{T}}_{21} = \begin{bmatrix} 0 & 0 \\ 0 & \mathsf{T}_{21} \end{bmatrix}, \qquad \mathsf{T} = \begin{bmatrix} 0 & \widetilde{\mathsf{T}}_{12} \\ \widetilde{\mathsf{T}}_{21} & 0 \end{bmatrix},$$

$$\mathsf{A} = \begin{bmatrix} \mathsf{A}_1 & 0 \\ 0 & \mathsf{A}_2 \end{bmatrix}, \qquad \mathsf{B} = \begin{bmatrix} \mathsf{B}_1 & 0 \\ 0 & \mathsf{B}_2 \end{bmatrix}, \qquad \mathsf{M}^{\Gamma} = \begin{bmatrix} \mathbf{M}_1^{\Gamma_1} & 0 \\ 0 & \mathsf{M}_2^{\Gamma_2} \end{bmatrix},$$

$$\underline{\mathbf{u}} = \begin{bmatrix} \underline{\mathbf{u}}_1 \\ \underline{p}_1 \\ \underline{\mathbf{u}}_2 \\ \underline{p}_2 \end{bmatrix}, \quad \underline{\mathbf{w}} = \begin{bmatrix} \underline{\mathbf{w}}_1 \\ \underline{s}_1 \\ \underline{\mathbf{w}}_2 \\ \underline{s}_2 \end{bmatrix}, \quad \underline{\boldsymbol{\lambda}} = \begin{bmatrix} \underline{\boldsymbol{\lambda}}_1 \\ \underline{\lambda}_2 \end{bmatrix}, \quad \underline{\mathbf{f}} = \begin{bmatrix} \underline{\mathbf{f}}_1 \\ \underline{\mathbf{f}}_2 \end{bmatrix}.$$

The algebraic counterpart of OS (5.12)–(5.16) reads

$$\underbrace{\begin{bmatrix} \mathsf{A} & 0 & \mathsf{B} \\ -\mathsf{B}\mathsf{T} & \mathsf{A} & \mathsf{B} \\ -\mathsf{M}^{\Gamma}\mathsf{T} & \mathsf{M}^{\Gamma}\mathsf{T} & \mathsf{M}^{\Gamma} \end{bmatrix}}_{\mathsf{G}} \underbrace{\begin{bmatrix} \underline{\mathbf{u}} \\ \underline{\mathbf{w}} \\ \underline{\boldsymbol{\lambda}} \end{bmatrix}}_{\mathbf{x}} = \underbrace{\begin{bmatrix} \underline{\mathbf{f}} \\ \mathbf{0} \\ \mathbf{0} \end{bmatrix}}_{\mathbf{b}}. \tag{5.17}$$

By introducing the Schur-complement matrix S of G with respect to the control variable $\underline{\boldsymbol{\lambda}}$

$$\begin{aligned} \mathsf{S} &= \mathsf{M}^{\Gamma}\left(\mathsf{I} - \begin{bmatrix} -\mathsf{T} & \mathsf{T} \end{bmatrix} \begin{bmatrix} \mathsf{A} & 0 \\ -\mathsf{B}\mathsf{T} & \mathsf{A} \end{bmatrix}^{-1} \begin{bmatrix} \mathsf{B} \\ \mathsf{B} \end{bmatrix}\right) \\ &= \mathsf{M}^{\Gamma}(\mathsf{I} - (\mathsf{T}\mathsf{A}^{-1}\mathsf{B})^2) \end{aligned} \tag{5.18}$$

and the vector

$$\underline{\boldsymbol{\psi}} = \mathsf{M}^{\Gamma}(\mathsf{I} - \mathsf{T}\mathsf{A}^{-1}\mathsf{B})\mathsf{T}\mathsf{A}^{-1}\underline{\mathbf{f}},$$

the Schur-complement system associated with (5.17) reads

$$\mathsf{S}\underline{\boldsymbol{\lambda}} = \underline{\boldsymbol{\psi}} \tag{5.19}$$

and it can be regarded as the discrete counterpart of the interface equations (5.16).

Since the mass matrix M^{Γ} is not singular, we can scale G by left-multiplying the last row of (5.17), or equivalently both sides of (5.19), by $(\mathsf{M}^{\Gamma})^{-1}$. This operation can in fact be regarded as a left preconditioning system (5.19) by the matrix M^{Γ}.

The solution of the Schur-complement system (5.19) can be efficiently computed by Krylov methods (specifically, we will use Bi-CGStab ([51])). First of all we compute the right hand side of (5.19) as described in Algorithm 5.1. Then, given the array $\underline{\boldsymbol{\lambda}}^{(k)}$ at the kth iteration of Bi-CGStab, the matrix vector product $\underline{\boldsymbol{\chi}}^{(k)} = \mathsf{S}\underline{\boldsymbol{\lambda}}^{(k)}$ is performed by Algorithm 5.2.

ALGORITHM 5.1 ($\underline{\boldsymbol{\psi}}$ evaluation). *Given* $\mathbf{f}_1$ *and* $\mathbf{f}_2$*, compute* $\underline{\boldsymbol{\psi}}$.

1. solve (5.12) and (5.13) using homogeneous Dirichlet data on the interfaces Γ_1 and Γ_2 and right hand sides $\underline{\mathbf{f}}_1$ and $\underline{\mathbf{f}}_2$, respectively;

TABLE 5.1
Summary of equivalent strong–weak–discrete–algebraic formulations of ICDD for Stokes-Darcy coupling

Continuous strong form of control problem	(3.2) (3.3) (3.4)
Continuous weak form of control problem	(3.6) (3.7) (3.4)
Discrete weak form of control problem	(4.7) (4.10)
Discrete weak Euler Lagrange equation	(5.7)
Discrete weak Optimality System (OS)	(5.12) (5.13) (5.14) (5.15) (5.16)
Algebraic OS	(5.17)
Schur complement form of OS	(5.19)

2. solve the dual problems (5.14) and (5.15);
3. compute

$$\underline{\boldsymbol{\psi}}^{(k)} = \begin{bmatrix} -\mathbf{T}_{12}\underline{\mathbf{u}}_2 + \mathbf{T}_{12}\underline{\mathbf{w}}_2 \\ \mathsf{T}_{21}\underline{p}_1 + \mathsf{T}_{21}\underline{q}_1 \end{bmatrix}.$$

ALGORITHM 5.2 (Schur-complement evaluation). *Given* $\underline{\boldsymbol{\lambda}}^{(k)}$*, compute* $\underline{\boldsymbol{\chi}}^{(k)} = \mathcal{S}\underline{\boldsymbol{\lambda}}^{(k)}$.

1. solve (5.12) and (5.13) using $\underline{\boldsymbol{\lambda}}_1^{(k)}$ and $\underline{\lambda}_2^{(k)}$ as Dirichlet data on the interfaces Γ_1 and Γ_2, and null right hand sides $\underline{\mathbf{f}}_1$ and $\underline{\mathbf{f}}_2$, respectively;
2. solve the dual problems (5.14) and (5.15);
3. compute

$$\underline{\boldsymbol{\chi}}^{(k)} = \begin{bmatrix} \underline{\boldsymbol{\lambda}}_1^{(k)} - \mathbf{T}_{12}\underline{\mathbf{u}}_2 + \mathbf{T}_{12}\underline{\mathbf{w}}_2 \\ \mathsf{T}_{21}\underline{p}_1 - \underline{\lambda}_2^{(k)} + \mathsf{T}_{21}\underline{q}_1 \end{bmatrix}.$$

For reader's convenience, we conclude this section by summarizing in Table 5.1 all the equivalent formulations of ICDD method for Stokes-Darcy coupling presented in the paper: from the initial continuous strong form of the control problem (3.2)–(3.4), to the final Schur-complement algebraic form (5.19) implemented in our codes.

6. Numerical results. We consider some 2D test cases in which the computational domain represents a vertical section of a volume. The coordinates in the plane are x and z.

Our aim is twofold. On one hand we want to numerically assess the robustness of ICDD versus the discretization parameters (h and p) as well as versus the overlap thickness

$$\delta = \min_{\mathbf{x}_1\in\Gamma_1,\ \mathbf{x}_2\in\Gamma_2} \mathrm{dist}(\mathbf{x}_1, \mathbf{x}_2) > 0 \tag{6.1}$$

(see Test 0 in Section 6.1).

On the other hand, we want to analyze the robustness of ICDD method with respect to variations of the physical properties in the porous medium and to compare numerical solutions obtained by ICDD with those computed by a Sharp Interface (SI) approach based on the interface conditions (2.9). The latter approach is called SI-BJS to underline the use of the Beavers–Joseph–Saffman interface condition $(2.9)_3$ (see Tests 1, 2, 3 in Sects. 6.2–6.5).

In all test cases both the Stokes and the Darcy problems are discretized either by stabilized $\mathbb{Q}_p - \mathbb{Q}_p$ (or $\mathbb{P}_p - \mathbb{P}_p$) (for $p = 1, 2, ...$) $hp-$FEM using the stabilization

techniques presented in [23, 25] for the Stokes equations and those proposed in [39] for the Darcy problem, or by $\mathbb{P}_2 - \mathbb{P}_1$ FEM as described in Section 4.

The coupled problems are solved by the ICDD method (3.2)–(3.4). The Bi-CGstab method is used to solve the Schur complement system (5.19) with a given stopping tolerance ϵ.

For simplicity, we consider matching meshes in Ω_{12} and the same polynomial degrees for velocity and pressure in the Stokes and Darcy subdomains. Nevertheless we warn the reader that different discretizations can be adopted inside different subdomains and non-matching grids can be designed on the overlap, as it has been proposed in [18] for the elliptic-elliptic coupling.

6.1. Test 0. Let us consider the Stokes-Darcy coupling (3.2)–(3.3) with non-homogenenous boundary conditions featuring the following exact solution:

$$\begin{aligned} \mathbf{u}_1(x,z) = \mathbf{u}_2(x,z) = &\quad \left[-\frac{\kappa}{\mu}\frac{\pi}{2} e^{\frac{\pi}{2}x} \sin\left(\frac{\pi}{2}z\right); -\frac{\kappa}{\mu}\frac{\pi}{2} e^{\frac{\pi}{2}x} \cos\left(\frac{\pi}{2}z\right) \right] \\ p_1(x,z) = p_2(x,z) = &\quad e^{\frac{\pi}{2}x} \sin\left(\frac{\pi}{2}z\right) \end{aligned} \tag{6.2}$$

in $\Omega = (0,1)\times(0,2)$ and with $\kappa = 1/10$ and $\mu = 1$. Notice that all the theory developed in the previous sections is still valid with non-homogeneous boundary conditions, provided that suitable liftings of the boundary data are considered.

The overlapping subdomains are defined as follows: $\Omega_1 = (0,1) \times (1-\delta/2, 2)$ and $\Omega_2 = (0,1) \times (0, 1+\delta/2)$, with $\delta > 0$, and the meshes are uniform and structured in both subdomains.

In Tables 6.1–6.2 we report, respectively, the number of ICDD iterations required to solve system (5.19) up to tolerance $\epsilon = 10^{-9}$ and the convergence rates with respect to h relative to the following errors:

$$\begin{aligned} e_{u,1} &= \|\mathbf{u}_1 - \mathbf{u}_{1h}\|_{H^1(\Omega_1)}, \quad e_{p,1} = \|p_1 - p_{1h}\|_{L^2(\Omega_1)}, \\ e_{u,2} &= \|\mathbf{u}_2 - \mathbf{u}_{2h}\|_{L^2(\Omega_2)}, \quad e_{p,2} = \|p_1 - p_{2h}\|_{H^1(\Omega_2)}. \end{aligned} \tag{6.3}$$

The errors are measured for h in the range $[1/80, 1/5]$ for different FEM discretizations.

The results of Table 6.3 refer to discretizations with stabilized $\mathbb{Q}_p - \mathbb{Q}_p$ elements for $p = 1, \ldots, 6$. Here we report the number of ICDD iterations, the value ($\inf J$) of the cost functional J defined in (4.10), attained at convergence, and the errors (6.3).

The numerical results of Tables 6.2–6.3 show that the theoretical convergence orders of $hp-$FEM are guaranteed by ICDD iterations. More precisely, if the exact solution is infinitely smooth (which is the case of solution (6.2)), algebraic convergence of order p with respect to h and exponential convergence with respect to p are observed for $\mathbb{Q}_p - \mathbb{Q}_p$ ($p \geq 1$), in both Stokes and Darcy domains.

The number of ICDD iterations shown in Tables 6.1 and 6.3 is independent of both h and p, for fixed δ, and the attained value $\inf J$ is about the square of the stopping tolerance, meaning that in exact arithmetics $\inf J = 0$.

In Table 6.4 we report the number of ICDD iterations required to solve system (5.19) up to tolerance $\epsilon = 10^{-9}$ versus the overlap thickness δ. Different situations are considered. The results of the first five rows refer to fixed uniform and structured discretizations in either simplices or quads; those of the second block are obtained again by considering uniform and cartesian grids, but the mesh size h varies and the overlap thickness δ coincides with h; those of the last row are obtained by designing a quasi-uniform mesh of quads of maximum size $h = 1/5$ outside the overlap Ω_{12}, and a

TABLE 6.1
Test 0. ICDD iterations vs. the mesh size h for different FEM discretizations. The exact solution is given in (6.2). The overlap thickness is fixed $\delta = 0.4$

h	stabilized $\mathbb{Q}_1 - \mathbb{Q}_1$	stabilized $\mathbb{P}_1 - \mathbb{P}_1$	stabilized $\mathbb{P}_2 - \mathbb{P}_2$	$\mathbb{P}_2 - \mathbb{P}_1$ (Stokes-compatible)
1/5	8	4	4	4
1/10	8	4	4	4
1/20	7	4	4	4
1/40	7	4	4	4
1/80	7	4	4	4

TABLE 6.2
Test 0. Estimated convergence orders vs. the mesh size h for different discretizations. The exact solution is given in (6.2)

Convergence orders for	$e_{u,1}$	$e_{p,1}$	$e_{u,2}$	$e_{p,2}$
stab. $\mathbb{Q}_1 - \mathbb{Q}_1$	1.715	1.810	1.513	1.575
stab. $\mathbb{P}_1 - \mathbb{P}_1$	1.002	1.553	1.086	0.999
stab. $\mathbb{P}_2 - \mathbb{P}_2$	2.009	2.004	1.595	1.991
$\mathbb{P}_2 - \mathbb{P}_1$ (Stokes compat.)	2.000	1.999	1.963	1.000

strip of flattened quads of height equal to (decreasing) δ and width equal to $h = 1/5$ in Ω_{12}.

The results of Tables 6.1, 6.3 and 6.4 show that the number of ICDD iterations is independent of the discretization parameters h and p, while it depends on the overlap thickness δ as $\#it = \mathcal{O}(\delta^q)$, for some q between $-1/2$ and -1. A similar behavior has been observed when ICDD has been applied to elliptic problems in [18] and to the Stokes equations in [19].

In this example, the quality of the solution is not affected by the choice of the overlap thickness δ, since the test solution does not feature internal layers.

The next test cases are devised to assess the robustness of ICDD with respect to physical parameters and to perform comparisons with the sharp interface approach with interface conditions (2.9).

6.2. Test 1: Beavers–Joseph experiment. This simple test case mimics the experiment presented by Beavers and Joseph in their seminal paper [3]. We consider the rectilinear flow of a viscous fluid through a 2D parallel channel formed by an impermeable upper wall and a permeable lower wall. The latter defines a nominal surface for the permeable material. A uniform pressure gradient is maintained in the longitudinal direction in both the channel and the permeable media. Following the classification introduced by Ene, Levy and Sanchez-Palencia ([22, 37]), this test involves "near parallel flows", i.e. flows for which ∇p in the porous domain is parallel to the nominal interface and the velocity inside the porous domain is much smaller than in the fluid domain.

We set $\Omega = (0, 0.25) \times (-0.075, 0)$ (in meters), while the nominal interface is at $z_\Gamma = -0.055$. Given the overlap thickness $\delta > 0$, the overlapping subdomains are $\Omega_1 = (0, 0.25) \times (z_\Gamma - \delta, 0)$ and $\Omega_2 = (0, 0.25) \times (-0.075, z_\Gamma)$, so that $\Gamma_1 = (0, 0.25) \times \{z_\Gamma - \delta\}$, $\Gamma_2 = (0, 0.25) \times \{z_\Gamma\}$, and the overlap is thought to be embedded in the Darcy domain.

The fluid is water with density $\rho = 10^3$ $[kg/m^3]$ and dynamic viscosity $\mu = 10^{-3}$ $[kg/(m\ s)]$. The porous medium is characterized by its intrinsic permeability $\boldsymbol{\kappa}$ $[m^2]$,

TABLE 6.3
Test 0. ICDD iterations, infimum of the cost functional J and errors vs. the polynomial degree p for stabilized $\mathbb{Q}_p - \mathbb{Q}_p$ discretization in both Stokes and Darcy subdomains. The exact solution is given in (6.2). The overlap thickness is fixed $\delta = 0.4 = 4h$

p	$\#it$	$\inf J$	$e_{u,1}$	$e_{p,1}$	$e_{u,2}$	$e_{p,2}$
1	6	3.851e-18	4.9476e-02	2.9216e-01	7.5562e-02	5.9257e-02
2	7	4.800e-21	1.1310e-03	2.7244e-03	9.5293e-03	8.2701e-03
3	6	5.443e-20	1.4271e-05	1.4246e-05	4.0982e-05	4.0601e-05
4	6	6.118e-21	1.6159e-07	2.1171e-07	8.4074e-07	8.0511e-07
5	6	1.291e-21	1.6171e-09	1.2331e-09	4.8940e-09	5.1440e-09
6	6	4.934e-22	1.9260e-11	1.2030e-11	1.0879e-10	9.8985e-11

TABLE 6.4
Test 0. ICDD iterations versus the overlap thickness δ

fixed $h = 0.04$	$\delta =$	$5h$	$4h$	$3h$	$2h$	h
stab. $\mathbb{P}_1 - \mathbb{P}_1$	$\#it$	6	8	10	14	21
fixed $h = 0.04$	$\delta =$	$5h$	$4h$	$3h$	$2h$	h
stab. $\mathbb{P}_2 - \mathbb{P}_2$	$\#it$	6	8	11	21	28
fixed $h = 0.04$	$\delta =$	$5h$	$4h$	$3h$	$2h$	h
$\mathbb{P}_2 - \mathbb{P}_1$ (Stokes compat.)	$\#it$	6	8	9	11	20
fixed $h = 0.04$	$\delta =$	$10h$	$8h$	$6h$	$4h$	$2h$
stab. $\mathbb{Q}_1 - \mathbb{Q}_1$	$\#it$	7	7	8	8	9
fixed $h = 0.2$	$\delta =$	$10h$	$8h$	$6h$	$4h$	$2h$
stab. $\mathbb{Q}_4 - \mathbb{Q}_4$	$\#it$	5	5	5	6	8
	$h = \delta =$	1/3	1/6	1/12	1/25	
stab. $\mathbb{P}_1 - \mathbb{P}_1$	$\#it$	4	8	14	22	
	$h = \delta =$	1/3	1/6	1/12	1/25	
stab. $\mathbb{P}_2 - \mathbb{P}_2$	$\#it$	5	10	20	41	
	$h = \delta =$	1/3	1/6	1/12	1/25	
$\mathbb{P}_2 - \mathbb{P}_1$ (Stokes compat.)	$\#it$	4	6	9	21	
	$h = \delta =$	2/9	2/17	2/33	2/65	2/129
stab. $\mathbb{Q}_1 - \mathbb{Q}_1$	$\#it$	7	8	9	10	14
uniform mesh in $\Omega \setminus \Omega_{12}$, $h = 0.2$. One strip of quads of size $\delta \times h$ in Ω_{12}						
stab. $\mathbb{Q}_4 - \mathbb{Q}_4$	$\delta =$	$1.e-2$	$2.e-3$	$1.e-3$	$2.e-4$	$1.e-4$
	$\#it$	11	32	44	60	67

that we suppose homogeneous and isotropic, i.e. $\boldsymbol{\kappa} = \kappa \mathbf{I}$, where $\kappa > 0$ and $\mathbf{I}$ is the identity tensor.

To guarantee a uniform pressure gradient we set $\mathbf{f}_1 = (1,0)^t$ $[kg/(m^2\ s^2)]$, we impose a parabolic inflow on the left-hand side:

$$\mathbf{u}_1 = \begin{cases} (-10^3 z(z+0.055), 0)^t\ [m/s] & \text{if } -0.055 \le y \le 0 \\ (0,0)^t\ [m/s] & \text{otherwise} \end{cases}$$

and $\mathbf{T}_1(\mathbf{u}_1, p_1) \cdot \mathbf{n} = (x - 0.25, (-2z - 0.055))^t$ $[kg/(m\ s^2)]$ on the right-hand side.

In the Darcy domain we impose an external force $\mathbf{f}_2 = \mathbf{0}$ and the following boundary data: $\mathbf{u}_2 \cdot \mathbf{n}_2 = 0$ on the bottom horizontal side, $p_2 = 0.25$ $[kg/(m\ s^2)]$ on the left vertical side $\{0\} \times (-0.075, -0.055)$ and $p_2 = 0$ on the right one $\{0.25\} \times$

$(-0.075, -0.055)$.

We experienced that the choice of δ affects the Stokes solution computed by the ICDD method, at the same time it is known (see, e.g., [47, 41, 33]) that an internal layer of thickness $\mathcal{O}(\sqrt{\kappa}) = \mathcal{O}(\varepsilon)$ occurs between the fluid and the porous domains. Thus, it seems meaningful to set $\delta = c\sqrt{\kappa}$, where $c > 0$ is a suitable constant, that may depend on the geometry of the porous medium.

With this choice of δ, the continuity condition $\mathbf{u}_1 = \mathbf{u}_2$ on Γ_1 imposed by ICDD method not only implies the continuity of the normal component of the velocity $(2.9)_1$ on Γ_1, but also the fulfillment of a Beavers–Joseph-like condition (6.4). In fact, let us set $\mathbf{u}_i = (u_i, v_i)^t$, for $i = 1, 2$, and adapt the Beavers–Joseph condition (2.10) to the particular situation of this example:

$$\frac{\partial u_1}{\partial z}(z_\Gamma^+) = \frac{\alpha_{BJ}}{\sqrt{\kappa}}(u_1(z_\Gamma^+) - u_2(z_\Gamma^-)), \tag{6.4}$$

where z_Γ^+ and z_Γ^- are suitable points close to z_Γ such that $z_\Gamma^+ \in \Omega_1$ and $z_\Gamma^- \in \Omega_2$.

Now we approximate the derivative on the left of (6.4) by a first-order finite difference scheme with step size $\delta = z_\Gamma^+ - z_\Gamma^-$:

$$\frac{u_1(z_\Gamma^+) - u_1(z_\Gamma^-)}{\delta} \simeq \frac{\alpha_{BJ}}{\sqrt{\kappa}}(u_1(z_\Gamma^+) - u_2(z_\Gamma^-)), \tag{6.5}$$

and we choose

$$\delta = \frac{\sqrt{\kappa}}{\alpha_{BJ}}. \tag{6.6}$$

By looking at z_Γ^+ (respectively, z_Γ^-) as the vertical coordinate of the interface Γ_2 (respectively, Γ_1) and by using (6.6), we conclude that the interface condition $u_1(z_\Gamma^-) = u_2(z_\Gamma^-)$ (that we impose in the ICDD method) can be regarded as an approximation of the Beavers–Joseph condition (6.4).

The idea of using an interfacial region of thickness $\delta \simeq \sqrt{\kappa}/\alpha_{OW}$ has been considered in [41, 42], where α_{OW} is a suitable constant depending on the porous medium. However, in that case the authors solve a Stokes problem with an additional term featuring a variable porosity in such a region, a Darcy model with Brinkman correction in the porous domain and impose (for this test case) the continuity of both the tangential velocity and its normal derivative at the interfaces.

As a matter of fact, ICDD forces the continuity of both components of the velocity on the lower interface Γ_1 and the continuity of the pressure on the upper one Γ_2, but the Stokes and the Darcy solutions may not coincide on the overlap. Nevertheless, the differences between the local solutions are small as shown in 5th and 6th columns of Table 6.8.

It is well known that the parameter α_{BJ} depends on the geometry of the porous material. The characterization of such parameter goes beyond the aim of this paper and for simplicity we consider $\alpha_{BJ} = 1$.

After setting $\delta = \sqrt{\kappa} = \varepsilon$, we compute numerical solutions of this test case for $\kappa = 10^{-6},\ 10^{-8},\ 10^{-10}$. Larger values of κ would lead to a meaningless coupling since the characteristic length of the pores would become comparable with the characteristic length $x_s = 0.005$ of the Stokes domain (about the height of the channel). The solution of this problem is quite independent of the x variable, so we analyze its behavior at the fixed abscissa $\overline{x} = 0.15625$.

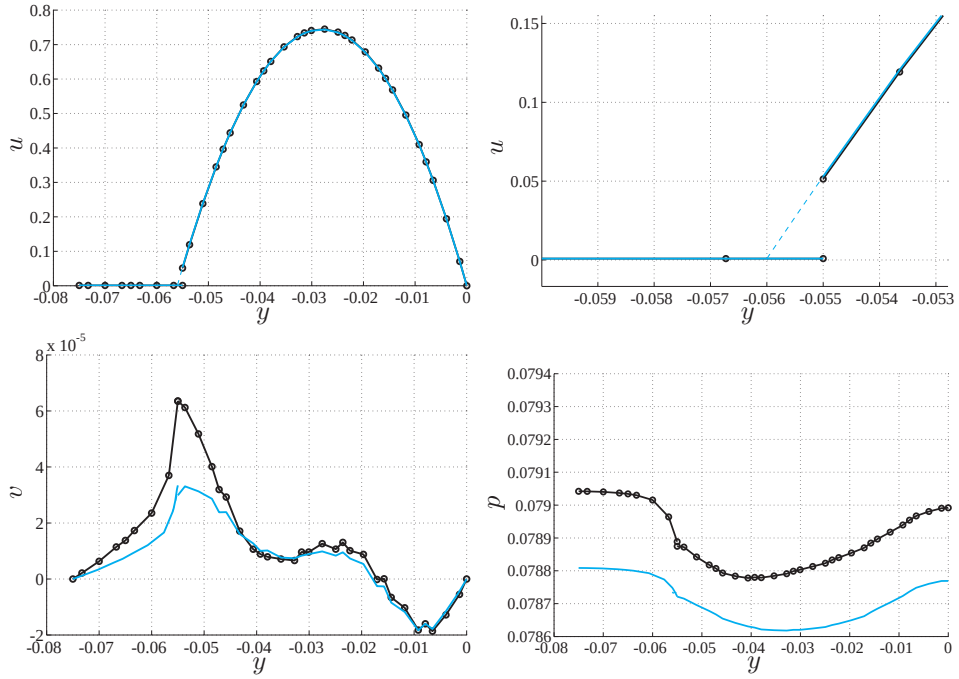

FIG. 6.1. *Test 1. Profiles of u (top), v (bottom left), and p (bottom right) at* $x = 0.15625$ *for* $\kappa = 10^{-6}\mathbf{I}$ *and SI-BJS approach (black line), ICDD with* $\delta = 10^{-3}$ *(light blue). The top right picture is a zoom of the top left one around the sharp interface* z_Γ*. The dashed line represents the first component of the Stokes velocity in the overlap region*

In Figure 6.1 we show the SI-BJS and ICDD solutions computed at $\overline{x}$ with $\kappa = 10^{-6}$. The SI-BJS solution is obtained by decomposing Ω with nominal interface in $z_\Gamma = -0.055$, while ICDD solution is found by setting $z_{\Gamma_1} = z_\Gamma - \delta$, $z_{\Gamma_2} = z_\Gamma$, and overlap thickness $\delta = \varepsilon = 10^{-3}$ (computed by (6.6)).

For smaller values of κ, the differences between SI-BJS and ICDD solutions are reported in Table 6.5, where $e_u(\overline{x})$, $e_v(\overline{x})$ and $e_p(\overline{x})$ are the relative difference in L^∞-norm between SI-BJS and ICDD solutions at $\overline{x} = 0.15625$, for $z < z_\Gamma$ (Darcy domain for sharp interface approach) and $z > z_\Gamma$ (Stokes domain for sharp interface approach). The results of Table 6.5 show that, when δ is chosen as in (6.6), ICDD and SI-BJS solutions match very well. In all these cases, as we can see in Table 6.6, we confirm the theoretical analysis performed in [3], [47], and [33], for which the order of magnitude of both components of the velocity in the Darcy domain is about $\mathcal{O}(\kappa) = \mathcal{O}(\varepsilon^2)$, while the tangential component of the Stokes velocity at the interface behaves like $\mathcal{O}(\sqrt{\kappa})$ when $\kappa \to 0$.

We fix now the permeability $\kappa = 10^{-8}$ and the thickness overlap $\delta = 10^{-4}$, but we consider three decompositions which differ one another for the position of the overlap with respect to the position z_Γ of the nominal interface Γ of SI-BJS:
- **lower** overlap, for which $z_{\Gamma_1} = z_\Gamma - \delta$ and $z_{\Gamma_2} = z_\Gamma$;
- **medium** overlap, for which $z_{\Gamma_1} = z_\Gamma - \delta/2$ and $z_{\Gamma_2} = z_\Gamma + \delta/2$;
- **upper** overlap, for which $z_{\Gamma_1} = z_\Gamma$ and $z_{\Gamma_2} = z_\Gamma + \delta$.

In Figure 6.2 we show the solutions at $\overline{x} = 0.15625$ for these three configurations, while in Table 6.7 we show the relative errors between ICDD and SI-BJS solutions in

TABLE 6.5

Test case 1. Relative maximum norm of the distance between SI-BJS and ICDD solutions at the coordinate $\overline{x} = 0.15625$. $e_u(\overline{x}) = \|u_{SI-BJS} - u_{ICDD}\|_{L^\infty(I)}/\|u_{SI-BJS}\|_{L^\infty(I)}$, $e_v(\overline{x}) = \|v_{SI-BJS} - v_{ICDD}\|_{L^\infty(I)}/\|v_{SI-BJS}\|_{L^\infty(I)}$, $e_p(\overline{x}) = \|p_{SI-BJS} - p_{ICDD}\|_{L^\infty(I)}/\|p_{SI-BJS}\|_{L^\infty(I)}$, *where* $I = \{\overline{x}\} \times (-0.075, -0.055)$ *in the Darcy domain and* $I = \{\overline{x}\} \times (-0.055, 0)$ *in the Stokes domain*

κ	Stokes domain			Darcy domain		
	$e_u(\overline{x})$	$e_v(\overline{x})$	$e_p(\overline{x})$	$e_u(\overline{x})$	$e_v(\overline{x})$	$e_p(\overline{x})$
10^{-6}	2.277e-03	5.339e-01	2.870e-03	2.868e-02	4.936e-01	3.014e-03
10^{-8}	2.628e-05	7.469e-03	1.154e-04	4.884e-02	4.314e-01	1.111e-04
10^{-10}	1.058e-05	1.364e-03	1.478e-05	4.920e-02	4.224e-01	3.597e-05

TABLE 6.6

Test case 1. Values of the first (u_i, $i = 1, 2$) *and second* (v_i, $i = 1, 2$) *component of the velocity at* $(\overline{x}, z_\Gamma)$ *with* $\overline{x} = 0.15625$ *and* $z_\Gamma = z_{\Gamma_2}$. $v_1 \neq v_2$ *since ICDD imposes continuity of* v *on the interface* Γ_1. *Values of* v_2 *of ICDD solution match well the corresponding values of the SI-BJS solution*

κ	ICDD solution				SI-BJS solution		
	u_1	u_2	v_1	v_2	u_1	u_2	$v_1 = v_2$
10^{-6}	5.30e-02	8.95e-04	2.94e-05	3.20e-05	5.13e-02	8.70e-04	6.32e-05
10^{-8}	5.48e-03	9.89e-06	3.29e-07	1.45e-07	5.46e-03	9.40e-06	1.85e-07
10^{-10}	5.50e-04	9.98e-08	2.36e-08	1.65e-09	5.50e-04	9.49e-08	1.95e-09
10^{-12}	5.50e-05	1.01e-09	2.06e-09	1.30e-11	5.50e-05	9.50e-10	1.98e-11

the $L^\infty-$ norm.

The ICDD solution obtained with the lower overlap is the closest one to the SI-BJS solution, however, differences among ICDD solutions with different overlaps are very small.

REMARK 6.1. ICDD provides continuous pressure on the interface Γ_2. On the other hand, because of the interface condition $(2.9)_2$, the pressure computed by SI-BJS approach shows a jump across the interface Γ that is proportional to μ/ρ, but independent of the pores scale ε.

The continuity of the pressure between the fluid and porous domains in the case of isotropic media and "near parallel flows" is advocated also in [47] and [34, 9].

6.3. Test 2: Cross-flow membrane filtration. This case addresses the coupling of Stokes and Darcy flows in a cross-flow membrane filtration setting. The data for this test case are taken from [29].

The domain is $\Omega = (0, 0.015) \times (-0.0075, 0)$ (in meters), the nominal interface is set at $z_\Gamma = -0.0055$. Given the overlap thickness $\delta > 0$, the overlapping subdomains are $\Omega_1 = (0, 0.015) \times (z_\Gamma - \delta, 0)$ and $\Omega_2 = (0, 0.015) \times (-0.0075, z_\Gamma)$ (see Fig. 6.3). The domain Ω_1 represents a part of channel closed on the top side where the fluid can flow through the vertical sides, while Ω_2 represents a vertical filter.

The fluid is water with density $\rho = 10^3$ $[kg/m^3]$ and dynamic viscosity $\mu = 10^{-3}$ $[kg/(m\ s)]$. The porous medium will be characterized by its intrinsic permeability $\boldsymbol{\kappa}$ $[m^2]$, that will be specified later.

We suppose that the fluid is subject to the gravitational force, thus $\mathbf{f}_1 = \mathbf{f}_2 = (0, -\rho g)^t$ $[kg/(m^2\ s^2)]$, where ρ is the density of the water and g the gravitational acceleration. The fluid enters into the domain Ω_1 through the vertical left-hand boundary, where we impose a parabolic inflow, on the top side of the domain Ω_1

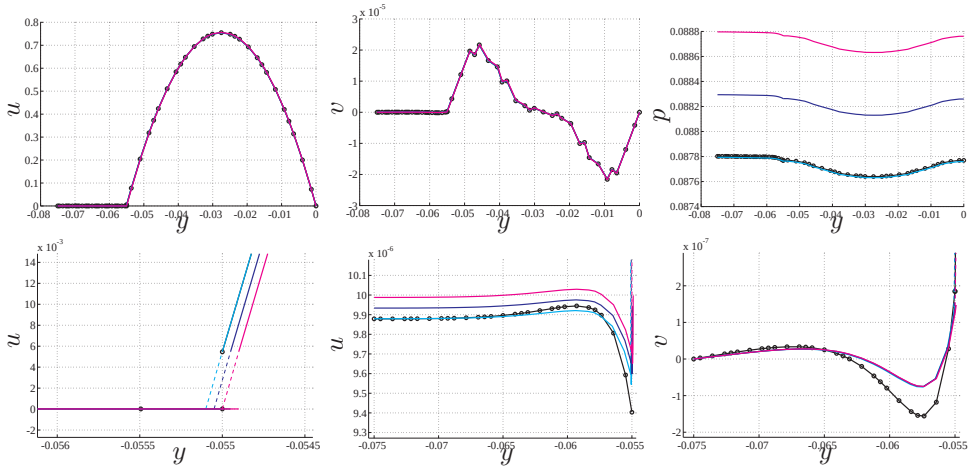

FIG. 6.2. *Test 1. Cuts of u, v, and p (top) at* $\overline{x} = 0.15625$ *for* $\kappa = 10^{-8}\mathbf{I}$*, computed by SI-BJS (black line) and ICDD (colored) with* $\delta = 10^{-4}$*: lower overlap (light blue), medium overlap (dark blue), and upper overlap (magenta). The bottom left and middle pictures are zooms of the first component of the velocity around the interface and inside the Darcy domain. The bottom right one is a zoom of the second component of the velocity in the porous domain. Dashed lines inside the overlap refer to the Stokes solutions*

TABLE 6.7

Test case 1. Relative maximum norm of the distance between SI-BJS and ICDD solutions on the cut $\overline{x} = 0.15625$ *for* $\kappa = 10^{-8}$*. The overlap (of fixed thickness) is located in three different positions around the nominal interface* Γ *of the sharp interface approach*

overlap	Stokes domain			Darcy domain		
	$e_u(\overline{x})$	$e_v(\overline{x})$	$e_p(\overline{x})$	$e_u(\overline{x})$	$e_v(\overline{x})$	$e_p(\overline{x})$
lower	2.628e-05	7.469e-03	1.154e-04	4.884e-02	4.314e-01	1.111e-04
medium	3.587e-03	1.707e-02	5.614e-03	1.965e-02	4.386e-01	5.647e-03
upper	7.220e-03	3.173e-02	1.133e-02	3.050e-02	4.362e-01	1.137e-02

we set the no-slip boundary conditions $\mathbf{u}_1 = \mathbf{0}$, while the fluid may leave the domain through the vertical right-hand boundary (denoted by $\partial\Omega_1^N$ in Fig. 6.3). Following the notations given in (3.2)–(3.3), the boundary data on $\partial\Omega_1^N \cup \partial\Omega_1^D$ can be summarized as follows:

$$\begin{aligned} &\mathbf{u}_1 = \mathbf{0} && \text{on } (0, 0.015) \times \{0\} \\ &\mathbf{u}_1 = \mathbf{0} && \text{on } \{0\} \times (-0.0055 - \delta/2, -0.005) \\ &\mathbf{u}_1 = (-16 \cdot 10^3 z(z + 0.005), 0)^t && \text{on } \{0\} \times (-0.005, 0) \\ &\mathbf{T}(\mathbf{u}_1, p_1) \cdot \mathbf{n}_1 = 9.8\rho z \mathbf{n}_1 && \text{on } \{0.015\} \times (-0.0055 - \delta/2, 0). \end{aligned} \tag{6.7}$$

Concerning the boundary conditions for the porous domain, we impose $\mathbf{u}_2 \cdot \mathbf{n}_2 = 0$ on the vertical sides $\partial\Omega_2^N$ to represent that an impervious material is present outside the domain, while we set $p_2 = -\rho g z$ on the bottom horizontal side $\partial\Omega_2^D$ to account for the presence of a stationary fluid below the porous domain.

The amount of flux filtering through the interface depends on the permeability of the porous media and on the boundary data imposed on the bottom horizontal side on the pressure.

Following the classification proposed by Ene, Levy and Sanchez-Palencia ([22, 37]), this test is numbered among "near normal flows", for which ∇p_2 has small

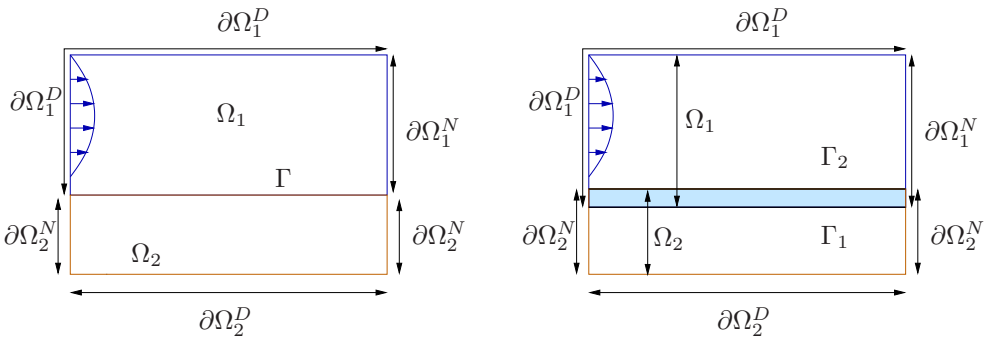

FIG. 6.3. *Test case 2. At left, the computational domain and its "physical" partition corresponding to different media. At right, the overlapping decomposition*

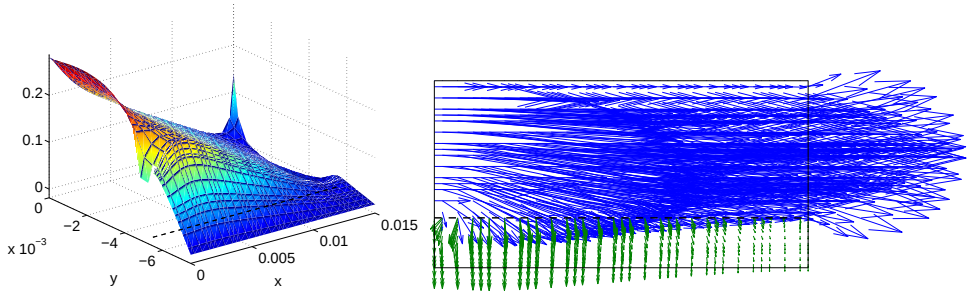

FIG. 6.4. *Test case 2. Hydrodynamic pressure (see (2.8)) and velocity field computed with* $\kappa = 10^{-7}\ m^2$ *and* $\delta = 3 \cdot 10^{-4}$*. For a better insight, the arrows in the right picture have been scaled by 10*

projection on the nominal interface and the order of magnitude of ∇p_2 is greater than that of ∇p_1.

To our knowledge, it has been neither experienced nor proved that either the Beavers–Joseph (2.10) or the Beavers–Joseph–Saffman $(2.9)_3$ conditions correctly describe this coupling. However, the latter condition is used in the literature (see, e.g. [36, 29]). We aim at comparing ICDD and SI-BJS approaches, studying both the quality of the solution and the associated computational costs.

We consider here several types of isotropic and homogeneous porous media characterized by different permeabilities.

In Figures 6.4 and 6.5 we show the pressure and the velocity field corresponding to $\kappa = 10^{-7}\ m^2$ and $\kappa = 10^{-13}\ m^2$.

In Fig. 6.6 we plot the profiles of u, v, and p at $\overline{x} \in \{3.75e{-}3,\ 7.5e{-}3,\ 1.125e{-}2\}$ when $\kappa = 10^{-7}$. Also in this test case we observe the close correspondence between ICDD and SI-BJS solutions. A quantitative comparison of the two solutions provides differences that behave like in Test 1 (see Tables 6.5) and shows that the tangential component of the Darcy velocity behaves like $\mathcal{O}(\kappa)$, while that of the Stokes velocity like $\mathcal{O}(\sqrt{\kappa})$, as in the case of "near parallel flows".

In Table 6.8 we report the number of ICDD iterations required to satisfy the stopping test on the residual up to tolerance $\epsilon = 10^{-9}$, the infimum of the cost functional J attained at convergence, and the norms

$$e_{\mathbf{u},\Omega_{12}} = \frac{\|\mathbf{u}_1 - \mathbf{u}_2\|_{L^2(\Omega_{12})}}{|\Omega_{12}|}, \qquad e_{p,\Omega_{12}} = \frac{\|p_1 - p_2\|_{L^2(\Omega_{12})}}{|\Omega_{12}|}, \tag{6.8}$$

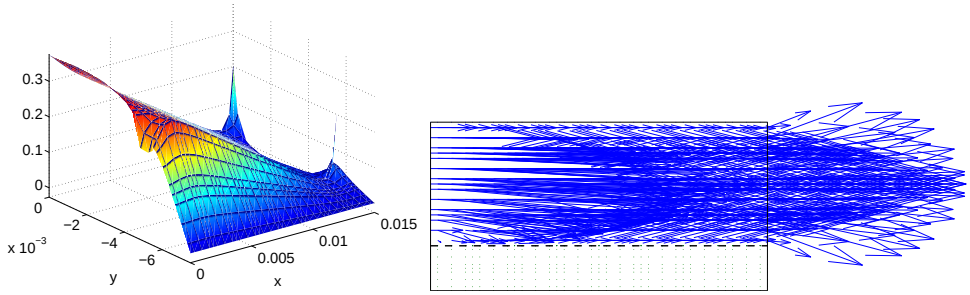

FIG. 6.5. *Test case 2. Hydrodynamic pressure (see (2.8)) and velocity field computed with* $\kappa = 10^{-13}$ m^2 *and* $\delta = 3 \cdot 10^{-7}$. *For a better insight, the arrows in the right picture have been scaled by 10*

TABLE 6.8

Test case 2. ICDD Iterations number, infimum of the cost functional, and errors on the overlap for different permeabilities. SI-BJS iterations number. Stabilized $\mathbb{Q}_4 - \mathbb{Q}_4$ *discretization in both subdomains.*

		ICDD				SI-BJS #it	
κ (m^2)	δ	#it	inf J	$e_{\mathbf{u},\Omega_{12}}$	$e_{p,\Omega_{12}}$	$P = S_s$	$P = S_d$
$1.e-7$	$3.e-4$	8	$1.02e-17$	$1.49e+0$	$5.47e-4$	13	17
$1.e-9$	$3.e-5$	5	$6.49e-20$	$3.24e-2$	$6.07e-4$	32	5
$1.e-11$	$3.e-6$	5	$3.09e-20$	$3.22e-4$	$8.23e-4$	33	4
$1.e-13$	$3.e-7$	5	$4.29e-20$	$3.23e-6$	$3.94e-4$	33	4

that measure the gap between Stokes and Darcy solutions on the overlap, normalized with respect to the size of the overlap (which is proportional to δ). We see that the gap on the velocity decays as κ, while that on the pressure is independent of κ.

The overlap thickness δ is set following (6.6), by choosing $\alpha_{BJ} = 1$. The discretization is almost fixed: we use stabilized $\mathbb{Q}_4 - \mathbb{Q}_4$ $hp-$FEM for both Stokes and Darcy equations. Outside the overlap, the mesh is almost uniform, with grid size $h = 2 \cdot 10^{-3}$ and $p = 4$. The overlap is discretized by one strip of flattened quad elements of size $h \times \delta$.

In Table 6.8, we also report the number of iterations required by Bi-CGstab to solve the Steklov-Poincaré equation associated with the Sharp Interface formulation of the Stokes–Darcy coupling with interface conditions (2.9), preconditioned by either the local Stokes Steklov-Poincaré operator (S_s) or the local Darcy Steklov-Poincaré operator (S_d) (see [21]).

It is evident that the convergence rate of ICDD is less sensitive to the permeability than that of the sharp interface approach and it does not require designing a suitable preconditioner.

Computational cost, comparison with sharp interface approach. As said above, one ICDD iteration corresponds to one Bi-CGStab iteration to solve the optimality system (5.12)–(5.16). Thus, it requires two matrix vector products (MVP), and each MVP requires solving two Stokes problems (like (5.12) and (5.14)) and two Darcy problems (like (5.13) and (5.15)). We can summarize that the

$$\text{cost of one ICDD iteration} = (4 \text{ Stokes} + 4 \text{ Darcy}) \text{ solves.}$$

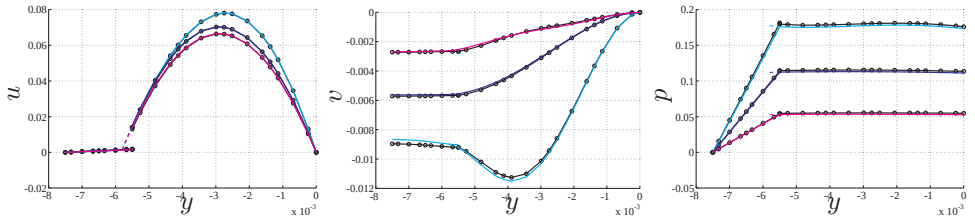

FIG. 6.6. *Test 2. Profiles of u (left), v (center), and hydrodynamic pressure $\tilde{p}$ (right) (see (2.8)), for SI-BJS solution (black line) and ICDD one (colored lines) at $\overline{x} = 3.75e-3$ (light blue), $\overline{x} = 7.5e-3$ (dark blue), $\overline{x} = 1.125e-2$ (magenta) when $\boldsymbol{\kappa} = 10^{-7}\mathbf{I}$. The thickness overlap for ICDD is $\delta = 3 \cdot 10^{-4}$*

Also the Steklov-Poincaré equation associated with the sharp interface approach can be solved by a Preconditioned Bi-CGstab method. In this case one MVP costs one Stokes plus one Darcy problem, while using the preconditioner costs one Stokes or one Darcy problem. Therefore, for SI-BJS, we have

$$\begin{aligned} \text{cost of one PBi-CGstab iteration} = \quad & \text{either (4 Stokes + 2 Darcy) solves} \\ & \text{or (2 Stokes + 4 Darcy) solves.} \end{aligned}$$

By comparing the number of iterations of Table 6.8, and in view of the fact that one ICDD iteration costs a little more than one SI-BJS iteration, we conclude that the computational costs of ICDD and SI-BJS are comparable.

Nevertheless, memory storage required by ICDD is less than the one required by SI-BJS. As a matter of fact, in ICDD, the Stokes matrices are the same for both primal and dual problems (and the same happens for Darcy), while in the case of SI-BJS, the preconditioner (either Stokes or Darcy) does not coincide with the matrix of the primal problem, in view of the different boundary conditions at the interface that characterize the direct local Steklov-Poincaré operator or its inverse (see [21] for a more in depth description of this approach).

Moreover, we highlight the simplicity of working with the interface conditions of the ICDD approach, versus the complexity of implementing the interface conditions (2.9), especially when the interface is not a straight line.

This test proves that the correspondence between SI-BJS and ICDD solutions is very good also for "near normal flows" and that ICDD method provides a very competitive approach to SI-BJS, in terms of both computational costs and ease of programming.

6.4. Test 3: Near normal flow. The domain is $\Omega = (0, 0.1) \times (0, 0.1)$ (in meters) and the nominal interface is set at $z_\Gamma = 0.08$ Given the overlap thickness $\delta > 0$, the overlapping subdomains are $\Omega_1 = (0, 0.1) \times (z_\Gamma - \delta, 0.1)$ and $\Omega_2 = (0, 0.1) \times (0, z_\Gamma)$.

The fluid is water as in the previous case and we consider homogenenous and isotropic porous media with permeability $\boldsymbol{\kappa} = \kappa\mathbf{I}$.

The fluid is subject to the gravitational force $\mathbf{f}_1 = \mathbf{f}_2 = (0, -\rho g)^T$ and it moves towards the bottom of the domain because the pressure on the bottom side is set lower than the equilibrium value. The water enters into the domain Ω_1 through its vertical sides, where we impose $\mathbf{T}(\mathbf{u}_1, p_1)\mathbf{n}_1 = g\rho(z - 0.1)\mathbf{n}_1$. On the top horizontal side of Ω_1 we set no-slip boundary conditions.

For what concerns the boundary conditions for the porous domain, we impose $\mathbf{u}_2 \cdot \mathbf{n}_2 = 0$ on the vertical sides of $\partial\Omega_2^N$, that means that an impervious material

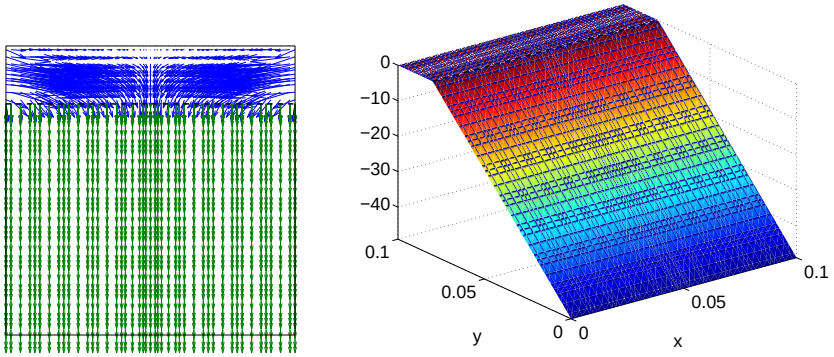

FIG. 6.7. *Test 3. Velocity field (left) and pressure (right) computed by ICDD with* $\delta = 10^{-4}$. *Discretization by stabilized* $\mathbb{Q}_4 - \mathbb{Q}_4$ *in both Stokes and Darcy domains. The permeability is* $\boldsymbol{\kappa} = \kappa \mathbf{I}$ *with* $\kappa = 10^{-8}$

is present outside the domain; while we set $p_2 = -0.95 g\rho(z - 0.1)$ on the bottom horizontal side $\partial\Omega_2^D$.

The pressure gradient in the Darcy domain is orthogonal to the interface (see Fig. 6.7) and this test case can be numbered among "near normal flows". The solution is symmetric with respect to the line $x = 0.05$, where the velocity is orthogonal to the interface.

The plot in Figure 6.7 (left) shows that the pressure gradient in the porous domain is very large with respect to that in the Stokes domain, where it is about 10^{-5}.

The adherence between ICDD and SI-BJS solutions is very high, as we can see from Fig. 6.8 and Tables 6.9– 6.10.

In Fig. 6.8 we report the profiles of the solutions at three different abscissas $\overline{x} \in \{0.02,\ 0.05,\ 0.08\}$ when $\kappa = 10^{-8}$. Numerical solutions corresponding to smaller values of the permeability behave similarly.

In Table 6.9 we report the relative difference in $L^\infty-$norm between ICDD and SI-BJS solutions. These errors are defined in the caption of Table 6.5.

In Table 6.10 we show the values of the two components of the velocity at the interface, again at $\overline{x} \in \{0.02,\ 0.05,\ 0.08\}$. Numerical results show that, in this case, for which $\nabla p_2 \perp \Gamma$, it holds:

$$u_1 = \mathcal{O}(\kappa^{3/2}), \quad u_2 = \mathcal{O}(\kappa^2), \quad v = \mathcal{O}(\kappa), \quad \kappa \to 0. \tag{6.9}$$

The number of iterations required by both ICDD and SI-BJS (preconditioned by the local Darcy Steklov-Poincaré operator) to converge up to a tolerance $\epsilon = 10^{-9}$ are: 3 when $\kappa = 10^{-8}$, 10^{-9}, and 10^{-10}, and 2 when $\kappa = 10^{-11}$.

6.5. Test 4: Isotropic non-homogeneous porous media. This case addresses the Stokes-Darcy coupling with isotropic non-homogeneous porous media and either straight or linear piecewise interface.

The domain is $\Omega = (0, 0.1) \times (0, 0.1)$ (in meters). First, the nominal interface is set at $z_\Gamma = 0.08$, in a second time we define a linear piecewise interface $z_\Gamma = z_\Gamma(x)$ (see Fig. 6.10). Given the overlap thickness $\delta > 0$, the overlapping subdomains are $\Omega_1 = \{(x, z) :\ x \in (0, 0.1),\ z \in (z_\Gamma(x) - \delta, 0.1)\}$ and $\Omega_2 = \{(x, z) :\ x \in (0, 0.1),\ z \in (0, z_\Gamma(x))\}$.

The fluid is water as in the previous case. The heterogeneity of the porous media

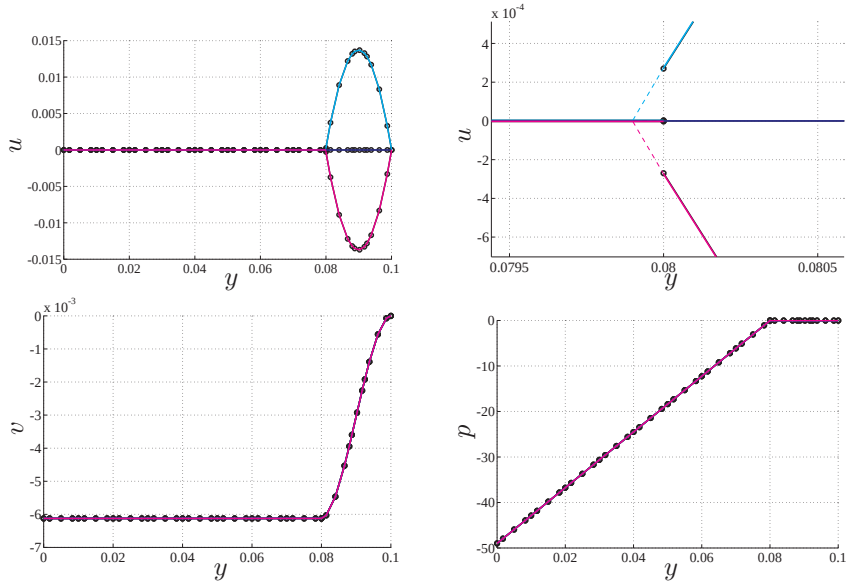

FIG. 6.8. *Test 3. Profiles of u (top), v (bottom left), and hydrodynamic pressure $\tilde{p}$ (bottom right) (see (2.8)), for SI-BJS solution (black line) and ICDD one (colored lines) at $\overline{x} = 0.02$ (light blue), $\overline{x} = 0.05$ (dark blue), $\overline{x} = 0.08$ (magenta) when $\kappa = 10^{-8}$*

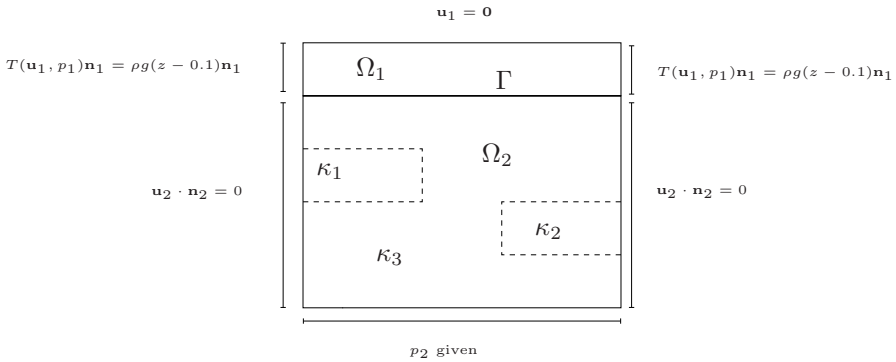

FIG. 6.9. *Test case 4. The computational domain and the data*

is measured in terms of its intrinsic permeability (see Fig. 6.9), by setting

$$\boldsymbol{\kappa}(x,z) = \begin{cases} 10^{-10}\mathbf{I}\ [m^2] & 0 \le x \le 0.04 \text{ and } 0.04 \le z \le 0.06, \\ 10^{-14}\mathbf{I}\ [m^2] & 0.06 \le x \le 0.1 \text{ and } 0.02 \le z \le 0.04, \\ 10^{-8}\mathbf{I}\ [m^2] & \text{elsewhere.} \end{cases}$$

Th external forces $\mathbf{f}_1 = \mathbf{f}_2$, as well as the boundary data are set as in Test case 3. As the previous one, also this test case is a "near normal flows". In Figure 6.10 the hydrodynamic pressure and the velocity field are shown: at left with a straight interface, at right with a piecewise linear interface. In both cases we set $\delta = 10^{-4}$ corresponding to $\delta = \sqrt{\kappa}$ with $\kappa = 10^{-8}$, that is the permeability in the region close to the interface.

ICDD solution is computed by discretization with stabilized $\mathbb{Q}_4 - \mathbb{Q}_4$ *hp*−FEM.

TABLE 6.9

Test case 3. Relative maximum norm of the distance between SI-BJS and ICDD solutions on the cuts $\overline{x} = 0.02,\ 0.05,\ 0.08$ for $\kappa = 10^{-8}$. e_u is not reported for $\overline{x} = 0.05$ since here u is about the machine precision

κ	Stokes domain			Darcy domain		
	$e_u(\overline{x})$	$e_v(\overline{x})$	$e_p(\overline{x})$	$e_u(\overline{x})$	$e_v(\overline{x})$	$e_p(\overline{x})$
$\overline{x} = 0.02$						
10^{-8}	2.822e-04	9.342e-05	1.281e-03	1.084e-02	1.426e-05	5.578e-06
10^{-9}	2.933e-04	7.561e-05	1.786e-04	8.770e-03	1.027e-05	5.978e-06
10^{-10}	2.704e-06	6.332e-06	1.272e-04	9.173e-03	1.021e-05	5.997e-06
10^{-11}	5.692e-05	8.507e-04	2.242e-03	8.085e-02	1.021e-05	5.999e-06
$\overline{x} = 0.05$						
10^{-8}		1.217e-04	9.414e-04		1.099e-05	5.632e-06
10^{-9}		6.390e-05	3.930e-05		1.023e-05	5.982e-06
10^{-10}		7.331e-06	8.758e-05		1.021e-05	5.998e-06
10^{-11}		7.722e-05	1.455e-04		1.021e-05	5.999e-06
$\overline{x} = 0.08$						
10^{-8}	2.822e-04	9.342e-05	1.281e-03	1.084e-02	1.426e-05	5.578e-06
10^{-9}	2.932e-04	7.563e-05	1.786e-04	8.668e-03	1.027e-05	5.978e-06
10^{-10}	2.809e-06	6.823e-06	1.270e-04	7.340e-03	1.021e-05	5.997e-06
10^{-11}	9.196e-05	3.545e-04	1.043e-03	5.716e-02	1.021e-05	5.999e-06

Convergence of ICDD up to tolerance $\epsilon = 10^{-9}$ is achieved in 3 iterations for straight interface and in 6 iterations for piecewise linear interface.

We stress once more the simplicity of implementing the ICDD approach when interfaces are not lines, since only conditions involving zeroth-order traces are involved.

Conclusions. In this paper we propose to solve the heterogeneous coupling between Stokes and Darcy equations by the ICDD method, a novel overlapping domain decomposition method that uses very simple interface conditions of Dirichlet type.

Several 2D test cases show the efficiency of this method, its robustness as well as the adherence of ICDD solution to that of the classical Sharp Interface approach with Beavers–Joseph–Saffman condition (SI-BJS). The overlap thickness is strictly connected with the characteristics of the porous medium and it is chosen equal to the size of the layer that occurs between the fluid and the porous domain.

The ICDD method features several interesting properties that make it preferable to other existing coupled methods like the one based on SI-BJS approach. Below we report some of them.

When the overlap thickness δ is set equal to the characteristic length scale of the pores $\varepsilon = \sqrt{\kappa}$, ICDD solutions are very close to SI-BJS ones, for both "near parallel flows" (classical test case of BJ) and "near normal flows".

The ICDD computational cost is comparable with that of SI-BJS, provided that the latter is preconditioned in an optimal way (either local Stokes or Darcy Steklov-Poincaré operator). On the contrary, the former one does not require any preconditioner to be efficient.

Simplicity in handling Dirichlet interface conditions is a strong point of ICDD, on the contrary interface conditions of SI-BJS involve both normal and tangential derivatives and they must accurately set up to take into consideration possible corners as well as non-straight interfaces.

TABLE 6.10
Test case 3. Values of the first (u_i, $i = 1, 2$) and second (v_i, $i = 1, 2$) component of the velocity at $(\overline{x}, z_\Gamma)$ with $z_\Gamma = z_{\Gamma_2}$

κ	ICDD solution			BJS solution		
	u_1	u_2	$v_1 = v_2$	u_1	u_2	$v_1 = v_2$
$\overline{x} = 0.02$						
10^{-8}	2.74e-04	2.75e-06	-6.12e-03	2.70e-04	2.78e-06	-6.12e-03
10^{-9}	8.26e-06	2.79e-08	-6.12e-04	8.66e-06	2.81e-08	-6.12e-04
10^{-10}	2.75e-07	2.79e-10	-6.12e-05	2.75e-07	2.82e-10	-6.12e-05
10^{-11}	8.63e-09	2.60e-12	-6.13e-06	8.71e-09	2.82e-12	-6.12e-06
$\overline{x} = 0.05$						
10^{-8}	-4.34e-13	1.72e-12	-6.12e-03	-4.18e-16	1.01e-14	-6.12e-03
10^{-9}	6.91e-13	4.37e-13	-6.12e-04	-3.48e-15	1.18e-15	-6.12e-04
10^{-10}	-4.68e-13	8.51e-14	-6.12e-05	-6.84e-16	1.16e-16	-6.12e-05
10^{-11}	2.20e-11	7.15e-14	-6.12e-06	-4.00e-16	1.16e-17	-6.12e-06
$\overline{x} = 0.08$						
10^{-8}	-2.74e-04	-2.75e-06	-6.12e-03	-2.70e-04	-2.78e-06	-6.12e-03
10^{-9}	-8.26e-06	-2.79e-08	-6.12e-04	-8.66e-06	-2.81e-08	-6.12e-04
10^{-10}	-2.75e-07	-2.80e-10	-6.12e-05	-2.75e-07	-2.82e-10	-6.12e-05
10^{-11}	-9.62e-09	-2.99e-12	-6.13e-06	-8.71e-09	-2.83e-12	-6.12e-06

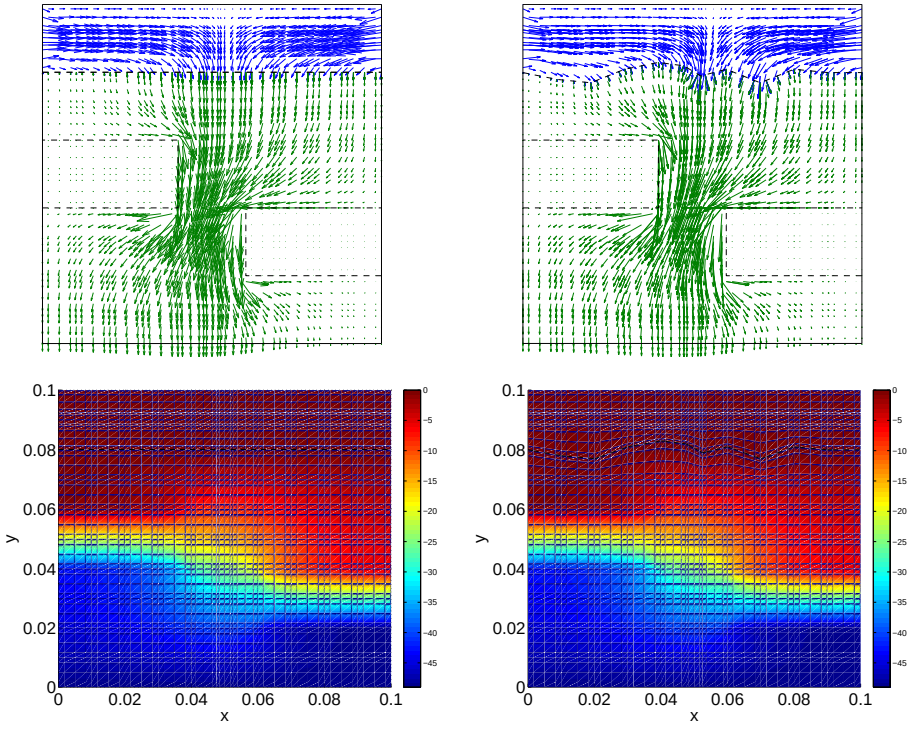

FIG. 6.10. *Test case 4. ICDD solution for $\kappa = 10^{-8} m^2$. At left with straight interface, at right with a piecewise interface*

The convergence rate of ICDD is independent of the discretization parameters. When the permeability is large, the number of iterations of ICDD is $\#it \simeq \mathcal{O}(\delta^q)$ with $-1 \leq q \leq -1/2$. However, since $\delta = \sqrt{\kappa}$, the previous estimate is not penalizing, because when κ is large, also δ is large.

REFERENCES

[1] L. Badea, M. Discacciati, and A. Quarteroni. Numerical analysis of the Navier-Stokes/Darcy coupling. *Numer. Math*, 115(2):195–227, 2010.

[2] J. Bear. *Dynamics of Fluids in Porous Media*. Dover Publications, Inc., New York, 1972.

[3] G.S. Beavers and D.D. Joseph. Boundary conditions at a naturally permeable wall. *J. Fluid Mech.*, 30:197–207, 1967.

[4] D. Boffi, F. Brezzi, and M. Fortin. *Mixed Finite Element Methods and Applications*. Springer-Verlag, 2013.

[5] H.C. Brinkman. A calculation of the viscous force exerted by a flowing fluid on a dense swarm of particles. *Appl. Sci. Res. A*, 1:27–34, 1947.

[6] C. Canuto, P. Gervasio, and A. Quarteroni. Finite-Element Preconditioning of G-NI Spectral Methods. *SIAM J. Sci. Comput.*, 31(6):4422–4451, 2009/10.

[7] C. Canuto, M. Y. Hussaini, A. Quarteroni, and T. A. Zang. *Spectral Methods. Fundamentals in Single Domains* . Springer, Heidelberg, 2006.

[8] C. Canuto, M. Y. Hussaini, A. Quarteroni, and T. A. Zang. *Spectral Methods. Evolution to Complex Geometries and Applications to Fluid Dynamics*. Springer, Heidelberg, 2007.

[9] T. Carraro, C. Goll, A. Marciniak-Czochra, and A. Mikelić. Pressure jump interface law for the Stokes-Darcy coupling: confirmation by direct numerical simulations. *J. Fluid Mech.*, 732:510–536, 2013.

[10] A. Çeşmelioğlu, V. Girault, and B. Rivière. Time-dependent coupling of Navier-Stokes and Darcy flows. *ESAIM: Mathematical Modelling and Numerical Analysis*, 47:539–554, 2013.

[11] M. Chandesris and D. Jamet. Jump condition and surface-excess quantities at a fluid/porous interface: a multi-scale approach. *Transp. Porous Med.*, 78:419–438, 2009.

[12] F. Cimolin and M. Discacciati. Navier-Stokes/Forchheimer models for filtration through porous media. *Appl. Numer. Math.*, 72:205–224, 2013.

[13] M.R. Correa and A.F.D. Loula. A unified mixed formulation naturally coupling stokes and darcy flows. *Comput. Methods Appl. Mech. Engrg.*, 198:2710–2722, 2009.

[14] H. Darcy. *Les Fontaines Publiques de la Ville de Dijon*. Dalmont, Paris, 1856.

[15] M. Discacciati. *Domain Decomposition Methods for the Coupling of Surface and Groundwater Flows*. PhD thesis, Ecole Polytechnique Fédérale de Lausanne, Lausanne (CH), 2004.

[16] M. Discacciati. Preconditioning methods for the coupled Darcy/Stokes system. Technical report, Universitat Politècnica de Catalunya, 2014. In preparation.

[17] M. Discacciati, P. Gervasio, and A. Quarteroni. *Heterogeneous mathematical models in fluid dynamics and associated solution algorithms*, volume 2040 of *Lecture Notes in Mathematics*, chapter 2, pages 57–123. Springer, 2011. Lectures given at the C.I.M.E. Summer School held in Cetraro, July 2009. Edited by G. Naldi and G. Russo.

[18] M. Discacciati, P. Gervasio, and A. Quarteroni. The interface control domain decomposition (ICDD) method for elliptic problems. *SIAM J. Control Optim.*, 51(5):3434–3458, 2013.

[19] M. Discacciati, P. Gervasio, and A. Quarteroni. The interface control domain decomposition (ICDD) method for the Stokes problem. *J. Coupled Syst. Multiscale Dyn.*, 1(5):372–392, 2013.

[20] M. Discacciati, P. Gervasio, and A. Quarteroni. Interface Control Domain Decomposition (ICDD) Methods for Coupled Diffusion and Advection-Diffusion Problems. Technical report, MOX, Politecnico di Milano, 2013. Submitted.

[21] M. Discacciati and A. Quarteroni. Navier-Stokes/Darcy coupling: modeling, analysis, and numerical approximation. *Rev. Mat. Complut.*, 22(2):315–426, 2009.

[22] H.I. Ene and E. Sánchez-Palencia. Équations et phénomènes de surface pour l′écoulement dans un modèle de milieu poreux. *J. Mécanique*, 14:73–108, 1975.

[23] L.P. Franca and S.L. Frey. Stabilized finite element methods: II. The Incompressible Navier-Stokes Equations. *Comput. Meth. Appl. Mech. Engrg.*, 99:209–233, 1992.

[24] P. Gervasio, J.-L. Lions, and A. Quarteroni. Heterogeneous coupling by virtual control methods. *Numerische Mathematik*, 90(2):241–264, 2001.

[25] P. Gervasio and F. Saleri. Stabilized spectral element approximation for the Navier-Stokes equations. *Numerical Methods for Partial Differential Equations*, 14:115–141, 1998.

[26] P. Girault and P.A. Raviart. *Finite Element Methods for the Navier-Stokes Equations*. Springer-Verlag, Berlin, 1986.
[27] V. Girault and B. Rivière. DG approximation of coupled Navier-Stokes and Darcy equations by Beaver-Joseph-Saffman interface condition. *SIAM J. Numer. Anal.*, 47(3):2052–2089, 2009.
[28] R. Glowinski, Q.V. Dinh, and J. Periaux. Domain decomposition methods for nonlinear problems in fluid dynamics. *Comput. Methods Appl. Mech. Engrg.*, 40(1):27–109, 1983.
[29] N.S. Hanspal, A.N. Waghode, V. Nassehi, and R.J. Wakeman. Development of a predictive mathematical model for coupled Stokes/Darcy flows in cross-flow membrane filtration. *Chem. Eng. J.*, 149:132–142, 2009.
[30] T.J.R. Hughes, L.P. Franca, and M. Balestra. A new finite element formulation for computational fluid dynamics: V. Circumventing the Babuška-Brezzi condition: a stable Petrov-Galerkin formulation of the Stokes problem accommodating equal-order interpolations. *Comput. Meth. Appl. Mech. Engrg.*, 59:85–99, 1986.
[31] A.S. Jackson, I. Rybak, R. Helmig, W.G. Gray, and C.T. Miller. Thermodynamically constrained averaging theory approach for modeling flow and transport phenomena in porous medium systems: 9. Transition region models. *Advanced in Water Resources*, 42:71–90, 2012.
[32] W. Jäger and A. Mikelić. On the boundary conditions at the contact interface between a porous medium and a free fluid. *Ann. Scuola Norm. Sup. Pisa Cl. Sci.*, 23:403–465, 1996.
[33] W. Jäger and A. Mikelić. On the interface boundary condition of Beavers, Joseph and Saffman. *SIAM J. Appl. Math.*, 60(4):1111–1127, 2000.
[34] W. Jäger, A. Mikelić, and N. Neuss. Asymptotic analysis of the laminar viscous flow over a porous bed. *SIAM J. Sci. Comput.*, 22(6):2006–2028, 2001.
[35] I.P. Jones. Low Reynolds number flow past a porous spherical shell. *Proc. Camb. Phil. Soc.*, 73:231–238, 1973.
[36] W.J. Layton, F. Schieweck, and I. Yotov. Coupling fluid flow with porous media flow. *SIAM J. Numer. Anal.*, 40(6):2195–2218 (2003), 2002.
[37] T. Levy and E. Sánchez-Palencia. On boundary conditions for fluid flow in porous media. *Internat. J. Engrg. Sci.*, 13(11):923–940, 1975.
[38] J.-L. Lions and O. Pironneau. Algorithmes parallèles pour la solution de problèmes aux limites. *C. R. Acad. Sci. Paris Sér. I Math.*, t. 327:947–952, 1998.
[39] A. Masud and T.J.R. Hughes. A stabilized mixed finite element method for Darcy flow. *Comput. Methods Appl. Mech. Engrg.*, 191(39-40):4341–4370, 2002.
[40] E. Miglio, A. Quarteroni, and F. Saleri. Coupling of free surface and groundwater flows. *Computers & fluids*, 32:73–83, 2003.
[41] A. Ochoa-Tapia and S. Whitaker. Momentum transfer at the boundary between a porous medium and a homogeneous fluid I. Theoretical development. *Int. J. Heat Mass Transfer*, 38:2635–2646, 1995.
[42] A. Ochoa-Tapia and S. Whitaker. Momentum transfer at the boundary between a porous medium and a homogeneous fluid II. Comparison with experiment. *Int. J. Heat Mass Transfer*, 38:2647–2655, 1995.
[43] A. Quarteroni. *Numerical Models for Differential Problems*. Series MS&A, Vol. 2. Springer, Milano, 2009.
[44] A. Quarteroni and A. Valli. *Numerical Approximation of Partial Differential Equations*. Springer Verlag, Heidelberg, 1994.
[45] A. Quarteroni and A. Valli. *Domain Decomposition Methods for Partial Differential Equations*. The Clarendon Press, Oxford University Press, New York, 1999.
[46] B. Rivière and I. Yotov. Locally conservative coupling of Stokes and Darcy flows. *SIAM J. Numer. Anal.*, 42(5):1959–1977, 2005.
[47] P.G. Saffman. On the boundary condition at the interface of a porous medium. *Stud. Appl. Math.*, 1:93–101, 1971.
[48] M. Sahraoui and M. Kaviany. Slip and no-slip velocity boundary conditions at interface of porous, plain media. *International Journal of Heat and Mass Transfer*, 35:927–943, 1992.
[49] B.F. Smith, P.E. Bjørstad, and W.D. Gropp. *Domain Decomposition*. Cambridge University Press, Cambridge, 1996.
[50] A. Toselli and O. Widlund. *Domain Decomposition Methods – Algorithms and Theory*, volume 34 of *Springer Series in Computational Mathematics*. Springer-Verlag, Berlin, 2005.
[51] H.A. van der Vorst. *Iterative Krylov methods for large linear systems*, volume 13 of *Cambridge Monographs on Applied and Computational Mathematics*. Cambridge University Press, Cambridge, 2003.

MOX Technical Reports, last issues

Dipartimento di Matematica "F. Brioschi",
Politecnico di Milano, Via Bonardi 9 - 20133 Milano (Italy)

17/2014 Discacciati, M.; Gervasio, P.; Quarteroni, A.
Interface Control Domain Decomposition (ICDD) Method for Stokes-Darcy coupling

16/2014 Dede, L.; Jaggli, C.; Quarteroni, A.
Isogeometric numerical dispersion analysis for elastic wave propagation

15/2014 Esfandiar, B.; Porta, G.; Perotto, S.; Guadagnini, A;
Anisotropic mesh and time step adaptivity for solute transport modeling in porous media

14/2014 Dassi, F.; Formaggia, L.; Zonca, S.
Degenerate Tetrahedra Recovering

13/2014 Ballarin, F.; Manzoni, A.; Quarteroni, A.; Rozza, G.
Supremizer stabilization of POD-Galerkin approximation of parametrized Navier-Stokes equations

12/2014 Fumagalli, I; Parolini, N.; Verani, M.
Shape optimization for Stokes flow: a reference domain approach

11/2014 Taddei, T.; Quarteroni, A.; Salsa, S.
An offline-online Riemann solver for one-dimensional systems of conservation laws

10/2014 Antonietti, P.F.; Dedner, A.; Madhavan, P.; Stangalino, S.; Stinner, B.; Verani, M.
High order discontinuous Galerkin methods on surfaces

09/2014 Chen, P.; Quarteroni, A.
A new algorithm for high-dimensional uncertainty quantification problems based on dimension-adaptive and reduced basis methods

08/2014 Cattaneo, L; Zunino, P.
A computational model of drug delivery through microcirculation to compare different tumor treatments